

**Final Progress Report to  
NASA Marshall Space Flight Center**  
Dr. Robert Thom  
Non-Destructive Testing and Tribology Research Branch  
Mail code EH 13 MSFC ED 14  
Huntsville AL 35812

**COMPUTATIONAL ANALYSIS OF MISALIGNED HYBRID  
THRUST BEARINGS FOR ADVANCED CRYOGENIC TURBO  
PUMPS**

NASA Grant NAG8-1395  
**BULK-FLOW ANALYSIS OF CRYOGENIC FLUID HYDROSTATIC/HYDRODYNAMIC  
THRUST BEARINGS ( PHASE II )**

by  
**Dr. Luis San Andrés**  
Professor  
Turbomachinery Laboratory  
Mechanical Engineering Department,  
Texas A&M University  
College Station, TX 77845

January 2001

# TABLE OF CONTENTS

|   | <u>page</u> |
|---|-------------|
| EXECUTIVE SUMMARY   | i           |
| NOMENCLATURE  | iii         |
| LIST OF TABLES  | vii         |
| LIST OF FIGURES   | vii         |
| <br>  |             |
| <b>INTRODUCTION</b>   | 1           |
| <b>BULK FLOW ANALYSIS</b>   | 2           |
| Perturbation analysis of the flow field                             | 7           |
| Zeroth-order bulk-flow equations on the film lands                  | 8           |
| First-order bulk-flow equations on the film lands                   | 9           |
| Zeroth- and first-order flow equations at a bearing recess          | 10          |
| Fluid film axial force and restoring moments                        | 10          |
| Fluid film dynamic axial force and moment coefficients              | 11          |
| Force and moment coefficients at the statically aligned condition   | 13          |
| The numerical solution procedure                                    | 14          |
| <b>THE COMPUTER PROGRAM HYDROTHRUSTM</b>                            | 14          |
| <b>PREDICTIONS AND DISCUSSION</b>                                   | 15          |
| Force and moment coefficients for the aligned hybrid thrust bearing | 18          |
| Effect of shaft static misalignment on thrust bearing performance   | 19          |
| <b>CONCLUSIONS</b>  | 22          |
| <b>REFERENCES</b>   | 23          |
| <br>  |             |
| Figures 3-11  | 24-28       |

# COMPUTATIONAL ANALYSIS OF MISALIGNED HYBRID THRUST BEARINGS FOR ADVANCED CRYOGENIC TURBO PUMPS

## EXECUTIVE SUMMARY

The report details an extended computational bulk-flow analysis for prediction of the static and dynamic force and moment performance of angled injection, orifice-compensated hydrostatic / hydrodynamic thrust bearings. The motion of the cryogenic fluid within the thin film lands of a thrust bearing is governed by a set of bulk-flow mass and momentum conservation and energy transport equations. Mass flow conservation and a simple model for momentum transport within the hydrostatic bearing recesses are also accounted for. The bulk-flow model includes flow turbulence with fluid inertia advection, Coriolis and centrifugal acceleration effects on the bearing recesses and film lands. The cryogenic fluid properties are obtained from realistic thermophysical equations of state.

A perturbation analysis leads to zeroth-order nonlinear equations governing the fluid flow for the thrust bearing operating at a static equilibrium position with misalignment, and first-order linear equations describing the perturbed fluid flow for small amplitude shaft motions in the axial direction and shaft angulations around two principal axes. Numerical solution to the zeroth-order flow field equations renders the bearing flow rate, thrust load, restoring moments, drag torque and power dissipation. Solution to the first-order equations determines 27 force and moment coefficients, i.e. nine stiffness, nine damping and nine inertia coefficients due to shaft displacements and angulations. The computational method implements established algorithms and generic subprograms available from prior developments.

The enhanced Fortran90 program, HYDROTHRUSTM, runs as a console application on Windows 95/NT personal computers. The program, help files and examples are available through Texas A&M University Technology License Office.

The effects of shaft misalignment on the static and dynamic force and moment performance of a refrigerant hybrid thrust bearing are evaluated at an optimal operating condition. The results complement earlier predictions advanced in Phase I of the project. The axial force/displacement stiffness coefficient and the direct moment/angle stiffness coefficients show an optimum value for a certain load (recess pressure ratio) while the damping coefficient steadily increases with the applied load. As the misalignment angle increases, both moment and force coefficients due to shaft axial displacements and angulations also increase. A whirl frequency ratio equal to 0.50 is predicted for most operating conditions. That is, thrust hybrid bearings offer the same limited stability characteristics as hydrodynamic thrust bearings when undergoing self-excited shaft angular motions.

The analysis and computational capability to predict the performance of (flexure pivot) tilting pad hybrid bearings were not finalized due to lack of resources and inadequate planning. This important objective will be addressed in the near future with the support of the TAMU Turbomachinery Laboratory.

The lack of experimental data for the performance of hybrid thrust bearings under operating conditions similar to those of cryogenic turbo pumps continues to impair the validation of the advanced computational model. Rocket engine manufacturers will soon advance in the practice and implementation of an “all fluid film bearing technology,” thus releasing reliable test data to benchmark the model, and most importantly, demonstrating the superior performance of externally pressurized fluid film bearings under stringent and realistic operating conditions.

## NOMENCLATURE

|            |   |
|------------|---|
| $A_o$      | $(\mathbf{p}d_o^2/4)$ . Effective orifice area [m <sup>2</sup> ].   |
| $A_B$      | $\mathbf{p} (R_{out}^2 - R_{in}^2)$ . Bearing surface area [m <sup>2</sup> ].   |
| $A_R$      | $\frac{1}{2}Q_R (R_{Ro}^2 - R_{Ri}^2) = \frac{1}{2}Q_R D_R l_R$ . Recess (pocket) area [m <sup>2</sup> ].<br>$\bar{A}_R = A_R / R_*^2$  |
| $b_R$      | recess arc length [m]. $\bar{b}_R = b_R / R_*$  |
| $C_*$      | Nominal (minimum) film clearance [m].   |
| $C_p$      | Fluid specific heat [J/kg · °K]. $\bar{C}_p = C_p / C_{p*}$   |
| $C_d$      | Orifice discharge coefficient.  |
| $C_{ab}$   | Force and moment damping coefficients, $\mathbf{a}, \mathbf{b} = Z, \mathbf{f}_x, \mathbf{f}_y$   |
| $C_d$      | Orifice discharge empirical coefficient   |
| $D_{out}$  | $2\mathcal{R}_{out}$ . Bearing outer diameter [m].  |
| $D_{in}$   | $2\mathcal{R}_{in}$ . Bearing inner diameter [m].   |
| $D_R$      | $2\mathcal{R}_R$ . Recess center diameter [m].  |
| $d_o$      | Orifice diameter [m]  |
| $E_c$      | $\frac{U_*}{T_* C_{p*}}$ . Eckert (heat transfer) number.   |
| $F_Z$      | Fluid film axial force [N]. $\bar{F}_Z = F_Z / [A_B (P_s - P_a)]$   |
| $f_{S,B}$  | $a_M \left[ 1 + \left( c_M \frac{r_{S,B}}{H} + \frac{b_M}{Re_{S,B}} \right)^{e_M} \right];$ $a_M = 0.001375$<br>$b_M = 5 \cdot 10^5; c_M = 1 \cdot 10^4$<br>$e_M = \frac{1}{3}$ |
|            | Turbulent flow Moody's friction factors at shaft and bearing surfaces.  |
| $H, h$     | Film thickness [m], $H/C_*$   |
| $H_{pad}$  | Pad film thickness including radial ( $dR$ ) and circumferential ( $dq$ ) tapers.   |
| $H_B, H_S$ | convection heat flow coefficients on bearing and shaft surfaces<br>[watt/m <sup>2</sup> °K]. $\bar{H}_B = H_B / H_{B*}; \bar{H}_S = H_S / H_{S*}$                               |
| $H_R$      | Recess depth [m]. $h_R = H_R / C$   |

|                         |   |
|-------------------------|---|
| $h_z, h_{f_x}, h_{f_y}$ | $=l, -r \sin \mathbf{q}, r \cos \mathbf{q}$ . Film perturbations in axial and angular directions.   |
| $K_{ab}$                | Force and moment stiffness coefficients, $\mathbf{a}, \mathbf{b} = Z, \mathbf{f}_x, \mathbf{f}_y$   |
| $K_{eq}$                | Equivalent moment coefficient for stability prediction [Nm/rad].  |
| $L$                     | $(R_{out} - R_{in})$ . Bearing radial length [m].   |
| $l_R$                   | $(R_{Ro} - R_{Ri})$ . Recess radial length [m].   |
| $M$                     | Bearing mass flow rate [kg/s].  |
| $M_{Rin}, M_{Rout}$     | Mass flow rates through inner and outer diameters of bearing [kg/s].  |
| $M_R$                   | Mass flow through recess orifice [kg/s]. $\bar{M}_R = M_R / (\mathbf{r}_* U_* C R_*)$   |
| $M_X, M_Y$              | Restoring moments on thrust collar [N.m]  |
| $M_G$                   | $\oint_G \mathbf{r} H \bar{U} \cdot \bar{\mathbf{h}} dG$ . Mass flow from recess boundary into to film lands [kg/s]. $\bar{M}_G = M_G / (\mathbf{r}_* U_* C R_*)$ |
| $M_{ab}$                | Force and moment inertia coefficients, $\mathbf{a}, \mathbf{b} = Z, \mathbf{f}_x, \mathbf{f}_y$   |
| $N_{rec}$               | Number of hydrostatic recesses (pockets) on bearing pad.  |
| $N_{pad}$               | Number of pads on bearing.  |
| $P, \bar{P}$            | Fluid pressure [N/m <sup>2</sup> ], $(P - P_a) / (P_s - P_a)$ .   |
| $P_R, P_s$              | Recess pressure, supply pressure [N/m <sup>2</sup> ].   |
| $P_{Re}^-, P_{Re}^+$    | Edge recess pressures [N/m <sup>2</sup> ].  |
| $P_{Din}, P_{Dout}$     | Fluid pressures at inner and outer bearing diameters [N/m <sup>2</sup> ].   |
| $P_a$                   | Characteristic pressure, $\text{MIN}[P_{Din}, P_{Dout}]$ [N/m <sup>2</sup> ].   |
| $P_{dyn}$               | $\frac{1}{2} \mathbf{r} (\mathbf{W} R_R)^2$ . Pressure due to centrifugal inertia effect at pocket radius   |
| $Q_{BS}$                | $Q_B + Q_S$ . Radial heat flow through bearing, $Q_B = H_B(T - T_B)$ , and shaft, $Q_S = H_S(T - T_S)$ , surfaces [watt/m <sup>2</sup> ].                         |
| $R, r$                  | Radial coordinate [m], $R / R_*$ .  |
| $R_*$                   | $R_{out}$ . Characteristic bearing radius [m].  |
| $Re$                    | $(\mathbf{r}_* \mathbf{W} R_* C / \mathbf{m}_*)$ . Nominal circumferential flow Reynolds number.  |
| $Re_p$                  | $(\mathbf{r}_* U_* C / \mathbf{m}_*)$ . Nominal pressure flow Reynolds number.  |
| $Re_{p*}$               | $(Re_p C / R_*)$ . Nominal modified pressure flow Reynolds number.  |
| $Re_s$                  | $(\mathbf{r}_* \mathbf{w} C^2 / \mathbf{m}_* = \mathbf{s} Re_{p*})$ . Squeeze film Reynolds number.   |

|  |  |
|--|--|
| $Re_B, Re_S$   | $(\mathbf{r}H/\mathbf{m}) [U_R^2 + U_q^2]^{1/2}, (\mathbf{r}H/\mathbf{m}) [U_R^2 + (U_q - WR)^2]^{1/2}$<br>Flow Reynolds numbers relative to bearing and shaft surfaces. |
| $r_S, r_B$   | Roughness depths of shaft and bearing surfaces [m].  |
| $s$  | $R/R_R$ . Local radial coordinate from pocket radius.  |
| $t$  | Time [s].  |
| $T, \bar{T}$   | Temperature, $\bar{T} = T / T_s$   |
| $T_s$  | Fluid supply temperature [K].  |
| $T_B, T_S$   | bearing and shaft surface temperatures [K].  |
| $T_o$  | Shear induced torque on bearing surface [Nm]. $\bar{T}_o = T_o C / (\mathbf{m}_* U_* R_*^3)$   |
| $U_*$  | $C^2 (P_s - P_a) / \mathbf{m}_* R_*$ . Characteristic fluid flow velocity [m/s].   |
| $U_r, u_r$   | Bulk-flow radial velocity [m/s], $U_r / U_*$ .   |
| $U_q, u_q$   | Bulk-flow circumferential velocity [m/s], $U_q / U_*$ .  |
| $V_R$  | $[A_R(H+H_R)+V_{supply}]$ . Recess volume including supply line volume [m <sup>3</sup> ]. $\bar{V}_R = V_R / R_*^2 C$  |
| $W_Z$  | External axial load on bearing [N]. $\bar{W}_Z = W_Z / [A_B (P_s - P_a)]$  |
| $WFR$  | Whirl frequency ratio for shaft angular motions.   |
| $Z_{ab}$   | $(K_{ab} - \omega^2 M_{ab} + i \omega C_{ab})$ . Force and moment impedance coefficients,<br>$\mathbf{a}, \mathbf{b} = Z, \mathbf{f}_X, \mathbf{f}_Y$                    |
| $\mathbf{a}$   | Fluid inlet swirl ratio at recess.   |
| $\mathbf{b}_P$                                       | $+(1/r)(\mathbf{f}_r/\mathbf{f}_P)$ . Fluid compressibility coefficient [m <sup>2</sup> /N]. $\bar{\mathbf{b}}_P = DP_{sa} \mathbf{b}_P$                                 |
| $\mathbf{b}_T$                                       | $-(1/r)(\mathbf{f}_r/\mathbf{f}_T)$ . Fluid volumetric expansion coefficient [1/K].<br>$\bar{\mathbf{b}}_T = T_* \mathbf{b}_T$   |
| $DP_{sa}$  | $(P_s - P_a)$ . Characteristic differential pressure [N/m <sup>2</sup> ].  |
| $\Delta Z, \Delta \mathbf{f}_X, \Delta \mathbf{f}_Y$ | Shaft axial displacement and angular rotations about the X and Y axes.   |
| $d_{Ro}$   | $\frac{C_d A_o (2 \mathbf{r}_* [P_s - P_a])^{1/2}}{(\mathbf{r} U C R)_*}$ . Dimensionless feed orifice coefficient.  |
| $\mathbf{f}_X, \mathbf{f}_Y$                         | Shaft angular displacements (misalignments) about the X and Y axes.  |
| $\gamma$   | First order shear coefficients [see Reference 2].  |

|                  |   |
|------------------|---|
| $k_r = k_q$      | $1/2(k_S + k_B)$ . Turbulence shear factors in $(r, q)$ flow directions.                                |
| $k_S, k_B$       | $f_S \times Re_S, f_B \times Re_B$ . Turbulent shear parameters at shaft and bearing.                   |
| $r$              | Fluid density [ $\text{kg}/\text{m}^3$ ], $\bar{r} = r / r_*$ .   |
| $\mu$            | Fluid viscosity [ $\text{Ns}/\text{m}^2$ ], $\bar{m} = m / m_*$ .                                       |
| $q$              | Circumferential coordinate [rad].   |
| $Q_P$            | Angular extent of a bearing pad [rad].  |
| $Q_{l\_pad}$     | Leading edge of a bearing pad [rad].  |
| $Q_R$            | angular extent of hydrostatic recess (pocket) [rad].  |
| $X_{qu}, X_{qd}$ | Empirical recess-edge entrance loss coefficients in circumferential (upstream, downstream) direction.   |
| $X_{ri}, X_{ro}$ | Empirical recess-edge entrance loss coefficients in radial direction, inner and outer radii boundaries. |
| $t$              | $wt$ . Dimensionless time.  |
| $L, S$           | $WR_* / U_*; wR_* / U_*$ . Circumferential speed and whirl frequency numbers                            |
| $W, w$           | shaft rotational speed, excitation or whirl frequency [rad/s]   |

**Subscripts** refer to:

|        |   |
|--------|---|
| $o$    | Orifice in recess feed.                                     |
| $s, a$ | Refer to pressure supply and ambient conditions.            |
| $0$    | Zeroth-order variables.                                     |
| $a, b$ | $\{Z, f_X, f_Y\}$ . First-order variables or perturbations. |
| $R, e$ | Bearing recesses and edges (entrance).                      |
| $u, d$ | Upstream and downstream of recess.                          |
| $B, S$ | Refer to bearing and shaft (collar) surfaces.               |

Overbar denotes dimensionless variables.

## LIST OF TABLES

|   | <u>page</u>   |
|---|---|
| 1 | Hydrostatic thrust bearing for R134a compressor application. 16                                 |
| 2 | Definitions for dimensionless bearing performance parameters, force and moment coefficients. 17 |
| 3 | Bearing performance parameters at nominal operating clearance and aligned shaft collar. 18      |
| 4 | Predictions for aligned bearing with angled hydrostatic feed injection. 21                      |

## LIST OF FIGURES

|    | <u>page</u>  |
|----|--|
| 1  | Geometry of a hydrostatic / hydrodynamic thrust bearing 3  |
| 2  | Depiction of bearing with shaft angular misalignments 3  |
| 3  | Operating clearance, recess pressure ratio, and axial force coefficients ( $K_{ZZ}$ , $C_{ZZ}$ ) versus axial load for statically aligned bearing. 24  |
| 4  | Moment force coefficients ( $K_{\hat{f}_x \hat{f}_x}$ , $K_{\hat{f}_x \hat{f}_y}$ , $C_{\hat{f}_x \hat{f}_x}$ , $C_{\hat{f}_x \hat{f}_y}$ ) and whirl ratio versus axial load for statically aligned bearing. 24 |
| 5  | Minimum and maximum film and recess pressures versus shaft collar static misalignment angle ( $-\hat{f}_x R_{out} / C$ ). 25   |
| 6  | Mass flow rates through bearing inner and outer radii and recess flow rate versus shaft collar static misalignment angle ( $-\hat{f}_x R_{out} / C$ ). 25  |
| 7  | Axial load ( $F_Z$ ), drag torque ( $T_o$ ) and restoring moments ( $M_X$ , $M_Y$ ) versus shaft collar static misalignment angle ( $-\hat{f}_x R_{out} / C$ ). 26   |
| 8  | Synchronous (force) stiffness coefficients versus shaft collar static misalignment angle ( $-\hat{f}_x R_{out} / C$ ). 27  |
| 9  | Force damping coefficients versus shaft collar static misalignment angle ( $-\hat{f}_x R_{out} / C$ ). 27  |
| 10 | Synchronous moment stiffness coefficients versus shaft collar static misalignment angle ( $-\hat{f}_x R_{out} / C$ ). 28   |
| 11 | Moment damping coefficients versus shaft collar static misalignment angle ( $-\hat{f}_x R_{out} / C$ ). 28   |

# COMPUTATIONAL ANALYSIS OF MISALIGNED HYBRID THRUST BEARINGS FOR ADVANCED CRYOGENIC TURBO PUMPS

## INTRODUCTION

Hybrid (combination hydrostatic and hydrodynamic) journal and thrust bearings and damping seal bearings are currently used as radial support elements in state of the art cryogenic turbo pumps. These compact - low count part turbo pumps operate sub critically at exceedingly high shaft speeds (180 krpm) with pressure differentials as large as 550 bars (8,000 psi). Externally pressurized fluid film bearings and seals enable to carry safely large thrust and lateral loads with virtually no DN life limit, little friction and wear, provide accuracy of positioning, and render large direct stiffness and damping force coefficients for control of critical speeds and attenuation of undesirable vibrations. These features even allow unshrouded impellers, thus significantly increasing turbo pump reliability.

The development of analytical models and design tools and the testing of components address to the mandates of an "all-fluid-film- bearing" technology for advanced and less costly (per launching cost) turbo pumps. San Andrés (1990-1996) performed the thermohydrodynamic analyses and developed computer programs for prediction of the static and dynamic force response of radial fluid film bearings. The research addressed effectively the theoretical and practical issues related to the operation and dynamic performance of cryogenic fluid film bearings; namely high speeds and pressures, flow turbulence, fluid inertia, fluid compressibility, thermal effects, and two-phase flow phenomena. The computational predictions have been validated with test data from *process fluid* film bearings with mineral oils, water and air in regimes of operation ranging from laminar flow to turbulent flows, and including the transition zone to fully developed turbulence.

San Andrés (1998, 2000) advanced the original bulk-flow analysis of hybrid thrust bearings for cryogenic fluid applications. The model and computational program include the most important physical aspects paramount to the performance of turbulent flow fluid film bearings dominated by fluid inertia effects on the film lands and bearing recesses, and including a realistic thermo physical model and fluid properties. At high surface speeds, centrifugal forces could lead to sub ambient film pressures, induce lubricant cavitation or denude of fluid large areas of the bearing surface, thus significantly reducing the thrust bearing load capacity. Furthermore, large circumferential fluid speeds greatly affect the inertial pressure drop at the edges of the bearing recesses.

The performance of thrust bearing for a refrigerant (dual use) application was evaluated at two operating speeds and pressure drops. The computed results, presented in dimensionless form, evidenced consistent trends in the bearing performance characteristics. As the applied axial load increases, the bearing operating clearance and flow rate decrease while the recess pressures increase. The axial stiffness coefficient shows a maximum for a certain intermediate load (recess pressure ratio) while the damping coefficient steadily increases. The predictions show at low recess pressures (i.e. low loads) fluid inflow through the bearing inner diameter and sub ambient pressures just

downstream of the bearing recess edges. These effects are solely due to centrifugal and Coriolis fluid inertia forces at sufficiently large surface speeds.

The present analysis advances the original work to include the effects of static shaft misalignments and dynamic shaft angulations on the static and dynamic force and moment performance of hybrid thrust bearings. Mass flow conservation, momentum and transport bulk flow equations are presented and numerically solved for hybrid thrust bearings, pressurized face seals and hydrodynamic thrust bearings. A perturbation analysis of the flow equations renders first-order (linearized) flow equations for determination of the dynamic force and moment coefficients due to shaft axial motions and angulations about two orthogonal axes. The analysis renders nine stiffness, nine damping and nine inertia force/moment coefficients for routine engineering analysis and prediction using commercial rotordynamics computational programs. Formulae for the threshold speed of instability and whirl frequency ratio in aligned hybrid thrust bearings are advanced with important implications for the critical mass moment of inertia in compact rotors.

The numerical method of solution implemented follows well-known CFD – control volume procedures for staggered meshes. The features of the computer program developed are also detailed.

## BULK FLOW ANALYSIS

Figure 1 shows the geometry of a hybrid (hydrostatic/hydrodynamic) thrust bearing. The thrust bearing maybe composed of a single continuous ( $360^\circ$ ) pad with ( $N_{rec}$ ) recesses distributed around the bearing area, or a number of pads ( $N_{pad}$ ) separated by radial grooves. Each pad contains one or more recesses.

Figure 2 displays a runner (shaft) surface with angular static misalignment angles  $\{f_X, f_Y\}$  about the lateral axes ( $X, Y$ ), respectively. In general, the bearing film thickness is written as

$$H(R, \mathbf{q}, t) = h C_* = H_{pad}(R, \mathbf{q}) + R f_Y \cos \mathbf{q} - R f_X \sin \mathbf{q} \quad (1)$$

where  $C_*$  is a characteristic clearance, and  $H_{pad}$  is the pad clearance including circumferential ( $d\mathbf{q}$ ) and radial ( $d\mathbf{r}$ ) tapers [1, 2].

Consider the turbulent flow within the film lands of a hybrid (hydrostatic/hydrodynamic) thrust fluid film bearing. The bulk-flow equations of motion within the thin film lands and the perturbation analysis for description of the equilibrium flow (zeroth-order) and perturbed flow (first-order) due to small amplitude axial and angular motions of the shaft collar follow.

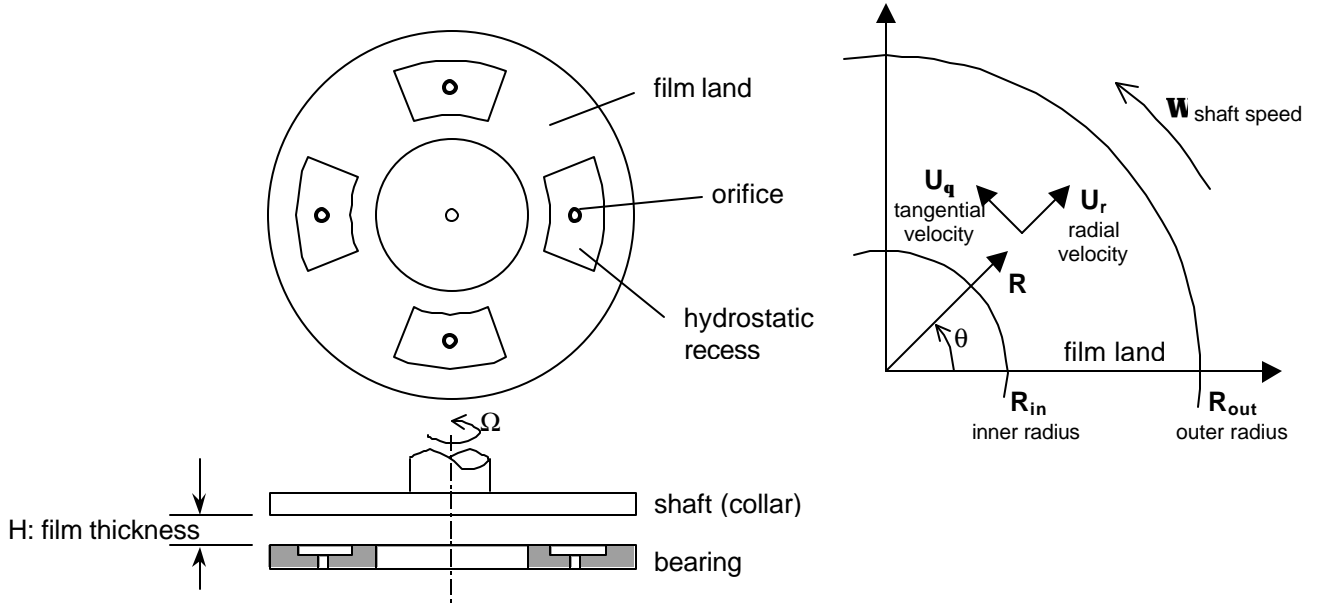


Figure 1. Geometry of a hydrostatic / hydrodynamic thrust bearing

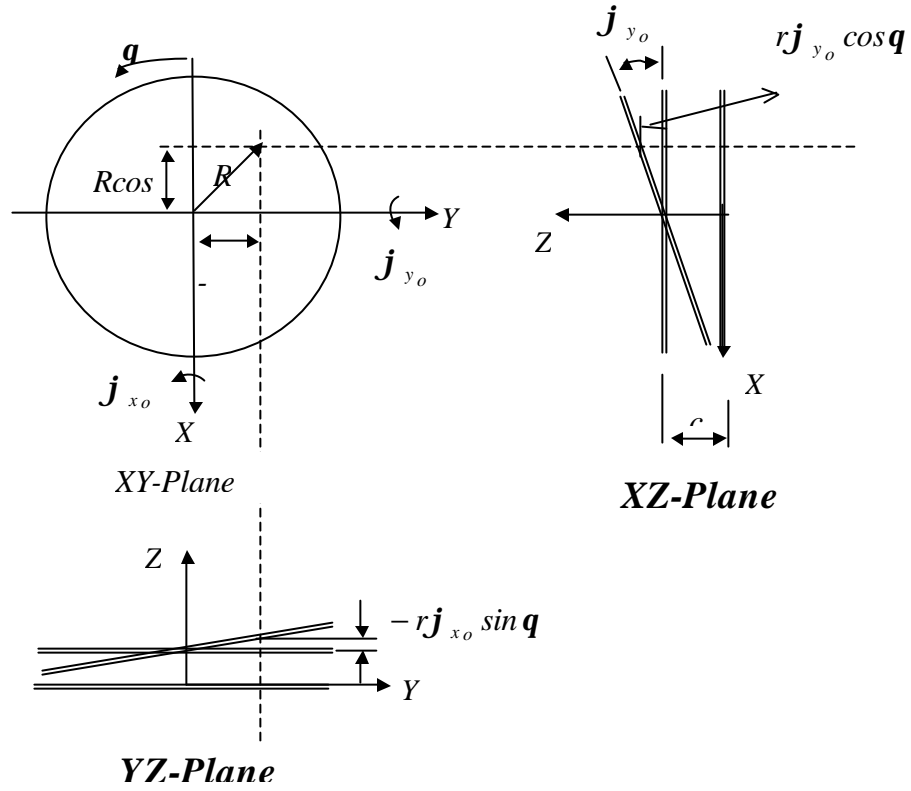


Figure 2. Depiction of bearing with shaft angular misalignments

The equations of mass, radial and circumferential momentum, and energy transport for the bulk-flow velocities, pressure and temperature on the bearing film lands are given in dimensionless form as [2,3]:

**continuity:**

$$\mathbf{s} \frac{\partial(\bar{\mathbf{r}} h)}{\partial \mathbf{t}} + \frac{1}{r} \frac{\partial(r \bar{\mathbf{r}} h u_r)}{\partial r} + \frac{1}{r} \frac{\partial(\bar{\mathbf{r}} h u_q)}{\partial \mathbf{q}} = 0 \quad (2.a)$$

**radial momentum:**

$$Re_{p^*} \left[ \mathbf{s} \frac{\partial(\bar{\mathbf{r}} h u_r)}{\partial \mathbf{t}} + \frac{1}{r} \frac{\partial(r \bar{\mathbf{r}} h u_r^2)}{\partial r} + \frac{1}{r} \frac{\partial(\bar{\mathbf{r}} h u_r u_q)}{\partial \mathbf{q}} - \frac{1}{r} \bar{\mathbf{r}} h u_q^2 \right] + \frac{\bar{\mathbf{m}}}{h} \mathbf{k}_r u_r = -h \frac{\partial \bar{P}}{\partial r} \quad (2.b)$$

**circumferential momentum:**

$$Re_{p^*} \left[ \mathbf{s} \frac{\partial(\bar{\mathbf{r}} h u_q)}{\partial \mathbf{t}} + \frac{1}{r} \frac{\partial(r \bar{\mathbf{r}} h u_r u_q)}{\partial r} + \frac{1}{r} \frac{\partial(\bar{\mathbf{r}} h u_q^2)}{\partial \mathbf{q}} + \frac{1}{r} \bar{\mathbf{r}} h u_r u_q \right] + \frac{\bar{\mathbf{m}}}{h} \left( \mathbf{k}_q u_q - \frac{1}{2} \mathbf{k}_s L r \right) = -\frac{h}{r} \frac{\partial \bar{P}}{\partial \mathbf{q}} \quad (2.c)$$

**energy transport:**

$$\left( \frac{Re_{p^*}}{E_c} \right) \bar{C}_p \left\{ \mathbf{s} \frac{\partial(\bar{\mathbf{r}} h \bar{T})}{\partial \mathbf{t}} + \frac{\partial(\bar{\mathbf{r}} h u_r \bar{T})}{\partial r} + \frac{1}{r} \frac{\partial(\bar{\mathbf{r}} h u_q \bar{T})}{\partial \mathbf{q}} \right\} + \left( \frac{Re_{p^*}}{E_c} \right) (\bar{H}_B + \bar{H}_S) \bar{T} = \left( \frac{Re_{p^*}}{E_c} \right) (\bar{H}_B \bar{T}_B + \bar{H}_S \bar{T}_S) + \bar{\mathbf{b}}_T h \bar{T} \left( \mathbf{s} \frac{\partial p}{\partial \mathbf{t}} + u_r \frac{\partial \bar{P}}{\partial r} + \frac{1}{r} u_q \frac{\partial \bar{P}}{\partial \mathbf{q}} \right) + \frac{1}{2} L h \frac{\partial \bar{P}}{\partial \mathbf{q}} + \frac{\bar{\mathbf{m}}}{h} \left[ \mathbf{k}_q \left( u_r^2 + u_q^2 + \frac{1}{2} L r u_q \right) \right] + \frac{\bar{\mathbf{m}}}{h} \left[ \mathbf{k}_s L r \left( \frac{1}{4} L r - u_q \right) \right] \quad (2.d)$$

Refer to the Nomenclature for a definition of all dimensionless variables. In the equations above,  $L = \frac{W R_*}{U_*}$  and  $\mathbf{s} = \frac{\mathbf{w} R_*}{U_*}$  are characteristic surface rotational speed and frequency

numbers, respectively;  $Re_{p^*} = \left( \frac{\mathbf{r}^* U_* C_*}{\mathbf{m}^*} \right) \frac{C_*}{R_*}$  is a nominal Reynolds Number based on the

pressure induced flow, and  $Re_s = Re_{p^*} \mathbf{s} = \left( \frac{\mathbf{r}^* \mathbf{w}^* C_*^2}{\mathbf{m}^*} \right)$  is the squeeze film Reynolds

number.  $E_c = \frac{U_*^2}{T_* C_{p^*}}$  is the Eckert heat transfer number, and  $(\bar{H}_B, \bar{H}_S)$  are

dimensionless convection heat transfer coefficients. The ratio  $\left( \frac{Re_{p^*}}{E_c} \right)$  refers to the effect of heat convection relative to mechanical shear dissipation.

The turbulent flow shear factors  $(\mathbf{k}_r = \mathbf{k}_q, \mathbf{k}_s)$  are defined in terms of the friction factors ( $f$ ) and Reynolds numbers ( $Re$ ) relative to the stationary bearing ( $B$ ) surface and shaft ( $S$ ) rotating surface. The Benedict-Web-Rubin equation of state is used to obtain cryogenic liquid properties  $(\mathbf{r}, \mathbf{m}, C_p)$  [4].

In a hydrostatic bearing, the fluid at pressure ( $P_s$ ) and temperature ( $T_s$ ) is supplied through orifice restrictors into the bearing pockets or recesses. The continuity equation at a hydrostatic recess establishes a balance among the mass flow through the feed orifice ( $\bar{M}_{R_i}$ ), the flow through the boundaries of the recess into the film lands ( $\bar{M}_\Gamma$ ), and the accumulation of fluid mass within the recess volume,  $V_R = [A_R (H + H_R) + V_{supply}]$ . The conservation of mass flows at a bearing recess is given in dimensionless form as,

$$\bar{M}_{R_i} = \bar{M}_{G_i} + \mathbf{s} \bar{\mathbf{r}}_{R_i} \left[ \frac{\partial \bar{V}_{R_i}}{\partial \mathbf{t}} + \bar{V}_{R_i} \left\{ \bar{\mathbf{b}}_P \frac{\partial \bar{P}}{\partial \mathbf{t}} - \bar{\mathbf{b}}_T \frac{\partial \bar{T}}{\partial \mathbf{t}} \right\}_{R_i} \right]; \quad i=1, \dots, N_{rec} \quad (3.a)$$

$$\text{where } \bar{M}_{R_i} = \mathbf{d}_{R_{o_i}} \left[ \bar{\mathbf{r}}_{R_{o_i}} (1 - \bar{P}_{R_i}) \right]^{1/2}, \text{ and } \bar{M}_{G_i} = \int_{B_i} \bar{\mathbf{r}} h \bar{\mathbf{u}} \cdot \bar{\mathbf{h}} d\bar{\mathbf{G}}_i \quad (3.b)$$

and  $\mathbf{d}_{R_i}$  as the orifice parameter. The energy transport balance within a bearing hydrostatic recess accounts for the mechanical energy dissipated by viscous shear, the heat-carry over (advection) from upstream conditions and the thermal mixing effects, i.e.

$$\left\langle \bar{C}_p \bar{V}_{R_i} \frac{\partial (\bar{\mathbf{r}} \bar{T})_{R_i}}{\partial \mathbf{t}} = \bar{C}_p \bar{M}_{R_i} \bar{T}_s - \int_{G_R} \bar{C}_p \bar{T} (\bar{\mathbf{r}} h \bar{\mathbf{u}}) \bar{\mathbf{h}} d\bar{\mathbf{G}}_{R_i} + \left( \frac{E_c}{Re_{p^*}} \right) \bar{T}_{o_{R_i}} \mathbf{L} \right\rangle_{i=1, \dots, N_{rec}} \quad (3.c)$$

where  $(\bar{P}, \bar{T})_R$  are the averaged pressure and temperature within the recess, and  $(\bar{\mathbf{r}}, \bar{\mathbf{b}}_P, \bar{\mathbf{b}}_T)_R$  are the dimensionless fluid density, fluid compressibility and thermal expansion coefficients, respectively.

The circumferential and radial pressure rises within the hydrostatic recesses are given, respectively, by

$$\left\langle \bar{P}_{Re}^- = \bar{P}_R + \bar{m}_R \frac{Q_{RR}}{2(h+h_R)^2} \left( \mathbf{k}_q u_q - \mathbf{k}_s \frac{Lr}{2} \right)_R \right\rangle_{i=1, \dots, N_{rec}} \quad (4.a)$$

$$\left\langle \bar{P} = \bar{P}_R + \bar{P}_{R_{dyn}} \left[ (s^2 - 1) \left\{ I + \left( \frac{u_{rR}}{s u_{qR}} \right)^2 \right\} - \frac{2 \bar{m} k_r u_{rR} r}{Re_{p^*} \bar{r} (h+h_R)^2 U_{qR}^2} \ln(s) \right] \right\rangle_{i=1, \dots, N_{rec}} \quad (4.b)$$

Equation (4.a) shows the circumferential increase in pressure downstream of a recess orifice as in a Rayleigh step bearing. Equation (4.b) shows the radial variation of recess pressure due to

- the viscous shear decreasing the pressure as the radius grows, i.e. towards the outer side of the bearing,
- centrifugal forces due to fluid rotation rising the pressure towards the outer radius of the recess; and,
- advection of fluid momentum in the radial direction reducing the pressure as the radius within the recess grows.

The entrance pressures to the film lands bounding the  $i_{th}$ -hydrostatic recess are expressed as,

$$\left\langle \bar{P}_{Re}^- = \bar{P}_{Re}^+ + \frac{(1+\mathbf{x})}{2} Re_{p^*} \bar{r}_e^- \left[ I - \left( \frac{\bar{r}_e^-}{\bar{r}_e^+} \right) \left( \frac{h}{h+h_R} \right)^2 \right] u_{r,q}^2 \right\rangle_{i=1, \dots, N_{rec}} \quad (5)$$

where  $\mathbf{x} = \{\mathbf{x}_i, \mathbf{x}_o, \mathbf{x}_{qu}, \mathbf{x}_{qd}\}$  are empirical entrance loss coefficients for the recess edges at its inner radius, outer radius, upstream and downstream circumferential directions, respectively. The sudden pressure drop is accounted for only if the fluid flow effectively enters the thin film lands.

The pressures at the inner and outer bearing radii are specified as,

$$\bar{P}(r_{in}) = \bar{P}_{Din}; \quad \bar{P}(r_{out}) = \bar{P}_{Dout} \quad (6)$$

These pressures are regarded as uniform or constant, and consequently, their variation under dynamic shaft motions is null.

In a 360° continuous film bearing or flat seal, the fluid pressure, temperature and velocities are singled valued in the circumferential direction, i.e.

$$\bar{P}, \bar{T}, u_r, u_q(r, \mathbf{q}, t) = \bar{P}, \bar{T}, u_r, u_q(r, \mathbf{q} + 2\mathbf{p}, t) \quad (7)$$

In a bearing pad, on the other hand, the pressures at the leading and trailing edges are specified radial function of the inner and outer radii pressures ( $\bar{P}_{D_{in}}, \bar{P}_{D_{out}}$ ).

Note that the momentum and energy flow equations applicable to the film lands are of hyperbolic character, and consequently, no exit conditions are required for the discharge temperature and fluid velocities at the bearing inner and outer radii. The balance of flow leaving the bearing recesses and entering the film lands provides the (inner) boundary conditions for the velocity fields within the thin film flow region, see equations (3).

### Perturbation analysis of the flow field

A perturbation analysis of the flow field for small amplitude axial and angular motions of the shaft collar about an equilibrium position follows. The analytical procedure renders sets of zeroth- and first-order flow equations for evaluation of the bearing static load capacity, drag torque, bearing and recess flow rates, and dynamic force and moment coefficients.

Consider the thrust collar to undergo small amplitude axial ( $DZ$ ) and angular rotations ( $Df_X, Df_Y$ ) at a frequency ( $w$ ) about an equilibrium position ( $h_0$ ). The film thickness is written as [5],

$$h(r, \mathbf{q}, t) = h_{pad_0}(r, \mathbf{q}) + \left( \frac{DZ}{C_*} \right) e^{iwt} + \left( \frac{R_*}{C_*} \right) r \left[ \{f_{Y_0} + Df_Y e^{iwt}\} \cos \mathbf{q} - \{f_{X_0} + Df_X e^{iwt}\} \sin \mathbf{q} \right] \quad (8)$$

with  $i = (-1)^{1/2}$ .  $h_{pad_0}$  and  $\{f_{X_0}, f_{Y_0}\}$  correspond to the pad film thickness and shaft static misalignment angles at the equilibrium condition<sup>1</sup>. Note that only the real part of the expression above is of importance in the analysis.

Using linear superposition, the equilibrium and perturbed films represented by zeroth- and first-order variables give,

$$h(r, \mathbf{q}, \mathbf{t}) = h_0 + \left\{ \left( \frac{DZ}{C_*} \right) h_Z + \left( \frac{R_*}{C_*} \right) h_{f_Y} + \left( \frac{R_*}{C_*} \right) h_{f_X} \right\} e^{it} \quad (9.a)$$

where  $\mathbf{t} = w t$ ,

$$h_0(r, \mathbf{q}) = h_{pad_0}(r, \mathbf{q}) + \left( \frac{R_*}{C_*} \right) r f_{Y_0} \cos \mathbf{q} - \left( \frac{R_*}{C_*} \right) r f_{X_0} \sin \mathbf{q} \quad (9.b)$$

$$\text{and} \quad h_Z = 1; \quad h_{f_Y} = r \cos \mathbf{q}; \quad h_{f_X} = -r \sin \mathbf{q} \quad (9.c)$$

<sup>1</sup> This equilibrium condition arises from the balance of the fluid film bearing reaction thrust (axial) force and restoring moments with the externally load and misalignment moments applied on the bearing.

Note that  $\left\{ \frac{d h_a}{d t} = i h_a e^{it} \right\}_{a=Z, f_x, f_y}$ . The flow pressure, temperature, bulk-flow velocities and shear factors are also expressed as the superposition of zeroth-order  $\{\mathbf{y}_0\}$  and first-order  $\{\mathbf{y}_a\}_{a=Z, f_x, f_y}$  flow fields describing the equilibrium and the perturbed fields, respectively, i.e.,

$$\mathbf{y} = \mathbf{y}_0 + \left\{ \left[ \frac{\Delta z}{C_*} \right] \mathbf{y}_z + \left[ \frac{R_*}{C_*} \right] \Delta \mathbf{f}_y \mathbf{y}_{f_y} + \left[ \frac{R_*}{C_*} \right] \Delta \mathbf{f}_x \mathbf{y}_{f_x} \right\} e^{it} \quad (10)$$

where  $\mathbf{y} = \{u_r, u_q, \bar{P}, \bar{T}, \bar{\mathbf{r}}, \bar{\mathbf{m}}, \mathbf{k}_r, \mathbf{k}_q, \mathbf{k}_s, \text{etc.}\}$ . Substitution of definitions (9) and (10) into the thin film land equations (2) leads to the zeroth- and first-order governing equations for the fluid bulk-flow.

### **Zeroth-order bulk-flow equations on the film lands**

#### **continuity:**

$$\frac{1}{r} \frac{\partial (r \bar{\mathbf{r}}_0 h_0 u_{r0})}{\partial r} + \frac{1}{r} \frac{\partial (\bar{\mathbf{r}}_0 h_0 u_{q0})}{\partial q} = 0 \quad (11.a)$$

#### **radial momentum:**

$$Re_{p^*} \frac{1}{r} \left[ \frac{\partial (r \bar{\mathbf{r}}_0 h_0 u_{r0}^2)}{\partial r} + \frac{\partial (\bar{\mathbf{r}}_0 h_0 u_{r0} u_{q0})}{\partial q} - \bar{\mathbf{r}}_0 h_0 u_{q0}^2 \right] + \frac{\bar{\mathbf{m}}_0}{h_0} \mathbf{k}_{0r} u_{r0} = -h_0 \frac{\partial \bar{P}_0}{\partial r} \quad (11.b)$$

#### **circumferential momentum:**

$$Re_{p^*} \frac{1}{r} \left[ \frac{\partial (r \bar{\mathbf{r}}_0 h_0 u_{r0} u_{q0})}{\partial r} + \frac{\partial (\bar{\mathbf{r}}_0 h_0 u_{q0}^2)}{\partial q} + \bar{\mathbf{r}}_0 h_0 u_{r0} u_{q0} \right] + \frac{\bar{\mathbf{m}}_0}{h_0} \left( \mathbf{k}_{q0} u_{q0} - \frac{1}{2} \mathbf{k}_{s0} L r \right) = -\frac{h_0}{r} \frac{\partial \bar{P}_0}{\partial q} \quad (11.c)$$

#### **energy transport:**

$$\left( \frac{Re_{p^*}}{E_c} \right) \bar{C}_{p0} \left\{ \frac{\partial (\bar{\mathbf{r}}_0 h_0 u_{r0} \bar{T}_0)}{\partial r} + \frac{1}{r} \frac{\partial (\bar{\mathbf{r}}_0 h_0 u_{q0} \bar{T}_0)}{\partial q} \right\} + \left( \frac{Re_{p^*}}{E_c} \right) (\bar{H}_{B0} + \bar{H}_{S0}) \bar{T}_0 = \left( \frac{Re_{p^*}}{E_c} \right) (\bar{H}_{B0} \bar{T}_{B0} + \bar{H}_{S0} \bar{T}_{S0}) + \bar{\mathbf{b}}_{r0} h_0 \bar{T}_0 \left( u_{r0} \frac{\partial \bar{P}_0}{\partial r} + \frac{1}{r} u_{q0} \frac{\partial \bar{P}_0}{\partial q} \right) + \frac{1}{2} L h_0 \frac{\partial \bar{P}_0}{\partial q} + \frac{\bar{\mathbf{m}}_0}{h_0} \left[ \mathbf{k}_{q0} \left( u_{r0}^2 + u_{q0}^2 + \frac{1}{2} L r u_{q0} \right) \right] + \frac{\bar{\mathbf{m}}_0}{h_0} \left[ \mathbf{k}_{s0} L r \left( \frac{1}{4} L r - u_{q0} \right) \right] \quad (11.d)$$

## First-order bulk-flow equations on the film lands

With  $h_a : \{ h_Z = 1; h_{f_Y} = r \cos \mathbf{q}; h_{f_X} = -r \sin \mathbf{q} \}$  for dynamic shaft axial motions and angulations about the (Y) and (X) axis, respectively. the perturbed flow equations are:

**continuity:**

$$i\mathbf{s} (\bar{\mathbf{r}}_0 h_a + \bar{\mathbf{r}}_a h_0) + \frac{1}{r} \frac{\partial}{\partial r} \left\{ r (\bar{\mathbf{r}}_a h_0 u_{r_0} + \bar{\mathbf{r}}_0 h_a u_{r_0} + \bar{\mathbf{r}}_0 h_0 u_{r_a}) \right\} + \frac{1}{r} \frac{\partial}{\partial \mathbf{q}} \left\{ \bar{\mathbf{r}}_a h_0 u_{q_0} + \bar{\mathbf{r}}_0 h_a u_{q_0} + \bar{\mathbf{r}}_0 h_0 u_{q_a} \right\} = 0 \quad (12.a)$$

**radial momentum:**

$$-h_0 \frac{\partial \bar{P}_a}{\partial r} = \mathbf{g}_{rh} h_a + \mathbf{g}_{rr} u_{r_a} + \mathbf{g}_{rq} u_{q_a} + \mathbf{g}_{rP} \bar{P}_a + \mathbf{g}_{rT} \bar{T}_a + \text{Re}_{p^*} \frac{1}{r} \left[ \frac{\partial (r \bar{\mathbf{r}}_0 h_0 u_{r_0} u_{r_a})}{\partial r} + \frac{\partial (\bar{\mathbf{r}}_0 h_0 u_{q_0} u_{r_a})}{\partial \mathbf{q}} + \bar{\mathbf{r}}_0 h_0 r \left( i\mathbf{s} + \frac{\partial u_{r_0}}{\partial r} \right) u_{r_a} + \bar{\mathbf{r}}_0 h_0 \left( \frac{\partial u_{r_0}}{\partial \mathbf{q}} - 2u_{q_0} \right) u_{q_a} \right] \quad \mathbf{a} = Z, \mathbf{f}_Y, \mathbf{f}_X \quad (12.b)$$

**circumferential momentum:**

$$-\frac{h_0}{r} \frac{\partial \bar{P}_a}{\partial \mathbf{q}} = \mathbf{g}_{qh} h_a + \mathbf{g}_{qr} u_{r_a} + \mathbf{g}_{qq} u_{q_a} + \mathbf{g}_{qP} \bar{P}_a + \mathbf{g}_{qT} \bar{T}_a + \text{Re}_{p^*} \frac{1}{r} \left[ \frac{\partial (r \bar{\mathbf{r}}_0 h_0 u_{r_0} u_{q_a})}{\partial r} + \frac{\partial (\bar{\mathbf{r}}_0 h_0 u_{q_0} u_{q_a})}{\partial \mathbf{q}} + \bar{\mathbf{r}}_0 h_0 \left( i\mathbf{s} r + u_{r_0} + \frac{\partial u_{q_0}}{\partial \mathbf{q}} \right) u_{q_a} + \bar{\mathbf{r}}_0 h_0 \left( r \frac{\partial u_{q_0}}{\partial r} + u_{q_0} \right) u_{r_a} \right] \quad \mathbf{a} = Z, \mathbf{f}_Y, \mathbf{f}_X \quad (12.c)$$

**energy transport:**

$$\left( \frac{\text{Re}_{p^*}}{E_c} \right) \bar{C}_{p_0} \left\{ \frac{\partial (\bar{\mathbf{r}}_0 h_0 u_{r_0} \bar{T}_a)}{\partial r} + \frac{1}{r} \frac{\partial (\bar{\mathbf{r}}_0 h_0 u_{q_0} \bar{T}_a)}{\partial \mathbf{q}} \right\} + \left( \mathbf{g}_{TT} + i\mathbf{s} \bar{\mathbf{r}}_0 h_0 \frac{\text{Re}_{p^*}}{E_c} \bar{C}_{p_0} \right) \bar{T}_a + \mathbf{g}_{Th} h_a + \mathbf{g}_{Tr} u_{r_a} + \mathbf{g}_{Tq} u_{q_a} + \left( \mathbf{g}_{TP} - i\mathbf{s} \bar{\mathbf{b}}_{T_0} h_0 \bar{T}_0 \right) \cdot \bar{P}_a - \frac{\mathbf{L}}{2} h_0 \frac{\partial \bar{P}_a}{\partial \mathbf{q}} \quad (12.d)$$

$$= \bar{\mathbf{b}}_{T_0} h_0 \bar{T}_0 \left( u_{r_0} \frac{\partial \bar{P}_a}{\partial r} + \frac{u_{q_0}}{r} \frac{\partial \bar{P}_a}{\partial \mathbf{q}} \right)$$

$\mathbf{a} = Z, \mathbf{f}_Y, \mathbf{f}_X$

San Andrés [2] lists the formulae for the first-order wall shear stress coefficients ( $\gamma$ 's).

### Zeroth- and first-order flow equations at a bearing recess

Perturbation of the recess mass flow and energy transport equations proceeds in the same manner. For the recess flows the linear combination of equilibrium and dynamic fields gives

$$\bar{M}_R = \bar{M}_{R0} + \left\{ \left[ \frac{DZ}{C^*} \right] \bar{M}_{RZ} + \left[ \frac{R^*}{C^*} \right] Df_Y \bar{M}_{Rf_Y} + \left[ \frac{R^*}{C^*} \right] Df_X \bar{M}_{Rf_X} \right\} e^{it} \quad (13)$$

The zeroth- and first-order equations for mass flow conservation at each recess are respectively,

$$\bar{M}_{R0i} = d_{R0i} \left[ \bar{r}_{R0i} (1 - \bar{P}_{R0i}) \right]^{1/2} = \bar{M}_{G0i} = \int_{G_i} \bar{r}_0 h_0 \bar{u}_0 \cdot \bar{\mathbf{h}} d\bar{G}_i, \quad i=1, \dots, N_{rec}, \quad (14)$$

and

$$\left\langle -C_{Ri}^P \bar{P}_{Rai} = \bar{M}_{Gai} + i \left( \mathbf{s} \bar{r}_{R0} \bar{A}_{R0} \right)_i h_{ai} + C_{Ri}^T \bar{T}_{Rai} \right\rangle_{i=1, \dots, N_{rec}} \quad \mathbf{a}=Z, \mathbf{f}_Y, \mathbf{f}_X \quad (15)$$

where

$$C_{Ri}^P = \left\{ \frac{\bar{M}_{R0}}{2(1 - \bar{P}_{R0})} [1 - \bar{b}_{PR} (1 - \bar{P}_{R0})] + i \left( \mathbf{s} \bar{V}_{R0} \bar{b}_{PR} \bar{r}_{R0} \right) \right\}_i \quad (16.a)$$

$$C_{Ri}^T = \bar{b}_{TR} \left\{ \frac{\bar{M}_{R0}}{2} - i \left( \mathbf{s} \bar{V}_{R0} \bar{r}_{R0} \right) \right\}_i; \quad i=1, \dots, N_{rec}$$

$$\text{with } \bar{M}_{Gai} = \int_{G_i} (\bar{r}_a h_0 \bar{u}_0 + \bar{r}_0 h_a \bar{u}_0 + \bar{r}_0 h_0 \bar{u}_a) \cdot \bar{\mathbf{h}} d\bar{G}_i; \quad i=1, \dots, N_{rec} \quad \mathbf{a}=Z, \mathbf{f}_Y, \mathbf{f}_X \quad (16.b)$$

as the first-order mass flow rates through the recess boundaries into the film lands.

The first-order energy transport equation at the recess and the pressure rise/drop equations at the recess edges are omitted for brevity.

### Fluid film axial force and restoring moments

Integration of the pressure field on the thrust collar surface (shaft) renders the axial force ( $F_Z$ ) reacting to an applied external load ( $W_Z$ ) and the restoring moments ( $M_Y, M_X$ ), i.e.

$$\begin{aligned}
F_Z &= -W_Z = \oint_{A_B} (P - P_a) R dR d\mathbf{q} \\
M_X &= - \oint_{A_B} (P - P_a) R \sin \mathbf{q} R dR d\mathbf{q} \\
M_Y &= \oint_{A_B} (P - P_a) R \cos \mathbf{q} R dR d\mathbf{q}
\end{aligned} \tag{17}$$

Recall that the pressure field is the superposition of zeroth- and first-order fields

$$\bar{P} = \frac{P - P_a}{P_s - P_a} = \bar{P}_0 + \left\{ \left[ \frac{DZ}{C_*} \right] \bar{P}_z + \left[ \frac{R_*}{C_*} \right] D\mathbf{f}_Y \bar{P}_{f_Y} + \left[ \frac{R_*}{C_*} \right] D\mathbf{f}_X \bar{P}_{f_X} \right\} e^{it} \tag{18}$$

due to the axial and angular changes in film thickness defined by

$$h(r, \mathbf{q}, \mathbf{t}) = h_0 + \left\{ \left[ \frac{DZ}{C_*} \right] h_z + \left[ \frac{R_*}{C_*} \right] h_{f_Y} + \left[ \frac{R_*}{C_*} \right] h_{f_X} \right\} e^{it} \quad \text{with } h_z = 1; \quad h_{f_Y} = r \cos \mathbf{q}; \quad h_{f_X} = -r \sin \mathbf{q}$$

Substitution of the pressure field, equation (18), into the force and moment equations (17) gives,

$$\begin{aligned}
F_Z &= (\Delta P_{sa} R_*^2) \oint_{A_B} \left[ \bar{P}_0 + \left\{ \left[ \frac{\Delta Z}{C_*} \right] \bar{P}_z + \left[ \frac{R_*}{C_*} \right] \Delta \mathbf{f}_Y \bar{P}_{f_Y} + \left[ \frac{R_*}{C_*} \right] \Delta \mathbf{f}_X \bar{P}_{f_X} \right\} e^{it} \right] r dr d\mathbf{q} \\
M_X &= - (\Delta P_{sa} R_*^3) \oint_{A_B} \left[ \bar{P}_0 + \left\{ \left[ \frac{\Delta Z}{C_*} \right] \bar{P}_z + \left[ \frac{R_*}{C_*} \right] \Delta \mathbf{f}_Y \bar{P}_{f_Y} + \left[ \frac{R_*}{C_*} \right] \Delta \mathbf{f}_X \bar{P}_{f_X} \right\} e^{it} \right] r^2 \sin \mathbf{q} dr d\mathbf{q} \\
M_Y &= + (\Delta P_{sa} R_*^3) \oint_{A_B} \left[ \bar{P}_0 + \left\{ \left[ \frac{\Delta Z}{C_*} \right] \bar{P}_z + \left[ \frac{R_*}{C_*} \right] \Delta \mathbf{f}_Y \bar{P}_{f_Y} + \left[ \frac{R_*}{C_*} \right] \Delta \mathbf{f}_X \bar{P}_{f_X} \right\} e^{it} \right] r^2 \cos \mathbf{q} dr d\mathbf{q}
\end{aligned} \tag{19}$$

where  $DP_{sa} = (P_s - P_a)$ .

### Fluid film dynamic axial force and moment coefficients

The bearing thrust force ( $F_Z$ ) and restoring moments ( $M_X, M_Y$ ) are also expressed as the superposition of equilibrium and dynamic forces and moments, i.e.

$$\begin{bmatrix} F_Z \\ M_Y \\ M_X \end{bmatrix} = \begin{bmatrix} F_{Z_0} \\ M_{Y_0} \\ M_{X_0} \end{bmatrix} - \begin{bmatrix} Z_{ZZ} & Z_{Zf_Y} & Z_{Zf_X} \\ Z_{f_Y Z} & Z_{f_Y f_Y} & Z_{f_Y f_X} \\ Z_{f_X Z} & Z_{f_X f_Y} & Z_{f_X f_X} \end{bmatrix} \begin{bmatrix} \Delta Z \\ \Delta \mathbf{f}_Y \\ \Delta \mathbf{f}_X \end{bmatrix} e^{i\omega t} \tag{20}$$

where the  $\{Z_{ab}\}_{a,b=Z,f_x,f_y}$  correspond to bearing impedances arising from the dynamic shaft motions. The dynamic stiffness (static stiffness and inertia) and damping coefficients are obtained from the real and imaginary parts of the impedance coefficients, i.e.

$$K_{ab} - \omega^2 M_{ab} + i \omega C_{ab} = Z_{ab} ; \mathbf{a}, \mathbf{b} = Z, f_Y, f_X \quad (21)$$

With the definitions forwarded, the bearing equilibrium forces and moments are given by

$$\begin{aligned} F_{Z_0} &= (DP_{sa} R_*^2) \oint_{A_B} \bar{P}_0 r dr d\mathbf{q} \\ M_{X_0} &= - (DP_{sa} R_*^3) \oint_{A_B} \bar{P}_0 r \sin \mathbf{q} r dr d\mathbf{q} \\ M_{Y_0} &= + (DP_{sa} R_*^3) \oint_{A_B} \bar{P}_0 r \cos \mathbf{q} r dr d\mathbf{q} \end{aligned} \quad (22)$$

and the dynamic bearing impedances are determined from

$$\begin{aligned} Z_{ZZ} &= - \left( \frac{DP_{sa} R_*^2}{C_*} \right) \oint_{A_B} \{ \bar{P}_Z \} r dr d\mathbf{q} , \quad Z_{Zf_Y} = - \left( \frac{DP_{sa} R_*^3}{C_*} \right) \oint_{A_B} \{ \bar{P}_{f_Y} \} r dr d\mathbf{q} , \\ Z_{Zf_X} &= - \left( \frac{DP_{sa} R_*^3}{C_*} \right) \oint_{A_B} \{ \bar{P}_{f_X} \} r dr d\mathbf{q} \\ Z_{f_X Z} &= + \left( \frac{DP_{sa} R_*^3}{C_*} \right) \oint_{A_B} \{ \bar{P}_Z \} r^2 \sin \mathbf{q} dr d\mathbf{q} , \quad Z_{f_X f_Y} = + \left( \frac{DP_{sa} R_*^4}{C_*} \right) \oint_{A_B} \{ \bar{P}_{f_Y} \} r^2 \sin \mathbf{q} dr d\mathbf{q} \\ Z_{f_X f_X} &= + \left( \frac{DP_{sa} R_*^4}{C_*} \right) \oint_{A_B} \{ \bar{P}_{f_X} \} r^2 \sin \mathbf{q} dr d\mathbf{q} \\ Z_{f_Y Z} &= - \left( \frac{DP_{sa} R_*^3}{C_*} \right) \oint_{A_B} \{ \bar{P}_Z \} r^2 \cos \mathbf{q} dr d\mathbf{q} , \quad Z_{f_Y f_Y} = - \left( \frac{DP_{sa} R_*^4}{C_*^3} \right) \oint_{A_B} \{ \bar{P}_{f_X} \} r^2 \cos \mathbf{q} dr d\mathbf{q} \\ Z_{f_Y f_X} &= - \left( \frac{DP_{sa} R_*^4}{C_*} \right) \oint_{A_B} \{ \bar{P}_{f_X} \} r^2 \cos \mathbf{q} dr d\mathbf{q} \end{aligned} \quad (23)$$

## Force and moment coefficients at the statically aligned condition

At the statically aligned shaft and bearing condition,  $f_{x_0} = f_{y_0} = 0$ , the force coefficients due to dynamic angulations and the moment coefficients due to axial displacements are null, i.e.

$$Z_{Zf_x} = Z_{Zf_y} = 0 = Z_{f_x Z} = Z_{f_y Z} = 0; \quad Z = \{K, C, M\} \quad (24)$$

A simple dynamic analysis for the stability of a rotating inertia determines the equivalent angular stiffness and whirl frequency ratio for shaft angulations as,

$$K_{eq} = \frac{K_{f_x f_x} C_{f_y f_y} + K_{f_y f_y} C_{f_x f_x} - K_{f_x f_y} C_{f_y f_x} - K_{f_y f_x} C_{f_x f_y}}{C_{f_x f_x} + C_{f_y f_y}} \quad (25)$$

$$WFR^2 = \left( \frac{w_n}{\Omega} \right)^2 = \frac{(K_{eq} - K_{f_x f_x})(K_{eq} - K_{f_y f_y}) - K_{f_y f_x} K_{f_x f_y}}{\Omega^2 (C_{f_x f_x} C_{f_y f_y} - C_{f_y f_x} C_{f_x f_y})}$$

The equations above may be used to determine the threshold speed of instability for shaft angular motions in a simple system.

Furthermore, at the aligned shaft condition, the following conditions also follow due to the rotational symmetry of the thrust bearing,

$$Z_{f_x f_x} = Z_{f_y f_y}; \quad Z_{f_y f_x} = -Z_{f_x f_y}; \quad Z = \{K, C, M\} \quad (26)$$

That is, the direct moment coefficients are symmetric and the cross-coefficients are anti-symmetric (due to the characteristic hydrodynamic effect). In this case, the matrix of dynamic impedances reduces to

$$[Z] = \begin{bmatrix} Z_{ZZ} & 0 & 0 \\ 0 & Z_{f_x f_x} & -Z_{f_x f_y} \\ 0 & Z_{f_x f_y} & Z_{f_x f_x} \end{bmatrix} \quad (27)$$

demonstrating the uncoupling between axial and angular shaft motions. The equivalent moment coefficient and whirl frequency ratio then reduce to

$$K_{eq} = K_{f_x f_x} + K_{f_x f_y} \frac{C_{f_x f_y}}{C_{f_x f_x}}; \quad WFR = \frac{K_{f_x f_y}}{\Omega C_{f_x f_x}} \quad (28)$$

## The solution procedure

Equations (11) and (14) describing the equilibrium flow field are solved using a control-volume numerical procedure. San Andrés details the discretization method and algorithm used in the computational analysis [2, 6]. The (discrete) first order flow fields defined by equations (12) and (15) are found once the zeroth-order fields are obtained. Bearing reaction forces and moments as well as dynamic force/moment coefficients follow from numerical integration of the flow fields on the bearing collar surface.

The interested reader should consult the works of Launder and Leschizer [7] and Van Dormaal and Raithby [8] for complete descriptions on the CFD procedure, including orders of accuracy and convergence.

## THE COMPUTER PROGRAM HYDROTHRUSTM

The HYDROTHRUSTM Fortran 90 computer program is an extension of the earlier HYDROTHRUST first released in 1998. Both programs run as console applications in a personal computer under the MS Windows operating system. The software includes a windows based help file (*hthrust.help*) and several examples featuring the options and capabilities of the program.

HYDROTHRUSTM calculates the static and dynamic force performance characteristics for the following bearing configurations:

1. hydrostatic / hydrodynamic thrust bearings with orifice compensation,
2. annular face seal with a pressure drop from inner diameter to outer diameter,
3. plain hydrodynamic thrust bearings.

Orifice injection is specified as axial or angled respect to the shaft rotational speed direction. The feed hole may be located anywhere within the recess, i.e. upstream or downstream of the middle plane.

HYDROTHRUSTM includes the following thermal models:

- adiabatic surfaces, i.e. insulated shaft and bearing surfaces.
- isothermal shaft at specified temperature and insulated (adiabatic) bearing.
- isothermal bearing at specified temperature and insulated (adiabatic) shaft.
- isothermal shaft and bearing surfaces.
- isothermal shaft and radial heat flow through bearing (stator).
- adiabatic shaft and radial heat flow through bearing (stator).

HYDROTHRUSTM calculates numerical predictions of:

- bearing flow rate or seal leakage,
- friction torque, power dissipation and temperature rise,
- load capacity if bearing minimum film clearance is given, or bearing film clearance if the external thrust load is given,
- restoring moments about two axes,

- three axial force stiffness, damping and inertia force coefficients due to collar displacements ( $\Delta Z$ ), and two shaft rotations ( $\Delta f_x, \Delta f_y$ ),
- three  $x$  two (=6) moment stiffness, damping and inertia force coefficients due to collar displacements ( $\Delta Z$ ), and two shaft rotations ( $\Delta f_x, \Delta f_y$ ).

Thus, the matrix of dynamic force coefficients comprises a total of 27 values corresponding to nine stiffness, nine damping and nine inertia force/moment coefficients.

The program interfaces with the NIST database to calculate the thermophysical properties of the following (single phase) cryogenic fluids:

(1) parahydrogen, (2) oxygen, (3) nitrogen, (4) methane.

Other fluids incorporated in the program are:

(5) water, (6) oil, (7) air, (12) barotropic fluid.

The help file *hthrust.help* gives a detailed description of the program operation and input/output calculation options.

## PREDICTIONS AND DISCUSSION

The analysis and computational program are applicable to a wide range of thrust bearing applications including operation at low speeds and feed pressures with viscous mineral oils (laminar flow bearings), and high speed hydrostatic / hydrodynamic thrust bearings for implementation in modern compact cryogenic liquid turbo pumps and state of the art turbomachinery using process fluid lubricants. To date, however, experimental results for these novel applications are not available in the open literature.

Table 1 presents the geometry and operating conditions of a six recess hydrostatic thrust bearing with R134a refrigerant for a commercial compressor application. San Andrés [2, 3] presents extensive predictions for a range of thrust loads at two operating speeds, 10 and 16 krpm, and pressure drops of 5.17 and 10.34 bars (75 and 150 psi), respectively. The operating film clearances ranged from 12.7 to 101.6  $\mu\text{m}$ . The computed predictions show the paramount effect of fluid inertia (on film lands and recess edges) on the performance characteristics of the thrust hybrid bearing.

The discussion concentrates on the effects of a static shaft misalignment ( $f_x$ ) on the performance characteristics of the hybrid thrust bearing operating with a nominal clearance ( $C$ ) of 0.508 mm. All calculations were performed with the full fluid inertia model, i.e. including fluid inertia effects at the film lands and recesses (area and edges interfacing with the film lands).

For reference in the discussion, Table 2 introduces the definitions for the dimensionless bearing performance characteristics.

**Table 1. Hydrostatic thrust bearing for R134a compressor application**  
Axial injection at mid plane of a recess.

| <b>Geometry, <math>N_{rec}=6</math></b>               |              | <b>SI dimensions</b>     | <b>English dimensions</b>  |
|---|--------------|--------------------------|--|
| Inner diameter  | $D_{in}$     | 89.13 mm                 | 3.51 inch  |
| Outer diameter  | $D_{out}$    | 126.8 mm                 | 4.99 inch  |
| Recess diameter                                       | $D_R$        | 108.6 mm                 | 4.28 inch  |
| Recess radial length                                  | $L_R$        | 11.68 mm                 | 0.46 inch  |
| Recess arc length                                     | $\Theta_R$   | 24°                      |  |
| Recess depth  | $H_R$        | 0.508 mm                 | 0.020 inch   |
| Film clearance (nominal)                              | $C$          | 0.051 mm                 | 0.002 inch   |
| Recess/Bearing area ratio                             |              | 0.25                     |  |
| Orifice diameter                                      | $d_o$        | 1.70 mm                  | 0.067 inch   |
| <u>Empirical parameters</u>                           |              |                          |  |
| Orifice discharge coefficient                         | $C_d$        | 0.80                     |  |
| Entrance loss coefficients,                           |              | 0.0, 0.0, 0.0, -         | $\mathbf{x}_{r_i}, \mathbf{x}_{r_o}, \mathbf{x}_{q_u}, \mathbf{x}_{q_d}$ |
|   |              | 0.5                      |  |
| Inlet swirl coefficient                               | $\mathbf{a}$ | 0.50                     |  |
| Bearing and collar relative surface roughness = 0.45% |              |                          |  |
| <b>Operating conditions</b>                           |              | <b>SI units</b>          | <b>English units</b>   |
| Speed   | $\Omega$     | 1,675 rad/s              | 16,000 rpm   |
| Supply temperature                                    | $T_s$        | 311 °K                   | 560 °R (100 °F)  |
| Supply pressure,                                      | $P_s$        | 24.10 bar                | 350 psia   |
| Exit pressure, $P_{Din}=P_{Dout}$                     | $P_a$        | 13.80 bar                | 200 psia   |
| Saturation pressure                                   | $P_{sat}$    | 9.63 bar                 | 139 psia   |
| Fluid properties                                      |              | <b>R134a</b> refrigerant |  |
| Density   | $\rho_a$     | 1210 kg/m <sup>3</sup>   | 75.54 lb/ft <sup>3</sup>   |
| Viscosity   | $\mu_a$      | 0.000198 Pa.s            | 0.0288<br>microReyns   |
| Fluid bulk modulus                                    | $(1/b_p)$    | 1,820 bar                | 26,667 psi   |
| Circumferential Reynolds number                       | $Re$         | 33,000                   |  |

**Table 2. Definitions for dimensionless bearing performance parameters, force and moment coefficients.**

|                                    | <u>Symbol</u>  | <b>Dimensionless parameter</b>   |
|------------------------------------|--|--|
| Pressure                           | $P$  | $p = \frac{P - P_a}{P_s - P_a}$  |
| Mass flow rate                     | $M$  | $\bar{M} = \frac{M}{N_{rec} C_d A_o [2 r_s (P_s - P_a)]^{1/2}}$  |
| Load                               | $F_Z$  | $\bar{F}_Z = \frac{F_Z}{F_*}; F_* = A_B (P_s - P_a)$   |
| Torque                             | $T_o$  | $\bar{T}_o = \frac{T_o}{T_{oT}}; T_{oT} = \left( 1 + 0.024 [0.4^2 Re_c]^{0.65} \right) \frac{m_s W A_B R_{out}^2}{C}$  |
| Moments                            | $M_X, M_Y$   | $\bar{M}_X = \frac{M_X}{F_* R_{out}}, \bar{M}_Y = \frac{M_Y}{F_* R_{out}}$   |
| Axial force stiffness coefficients | $K_{ZZ}, K_{Zf_Y}, K_{Zf_X}$   | $\bar{K}_{ZZ} = \frac{K_{ZZ} C}{F_*}, \bar{K}_{Zf_Y} = \frac{K_{Zf_Y} C}{F_* R_{out}}, \bar{K}_{Zf_X} = \frac{K_{Zf_X} C}{F_* R_{out}}$  |
| Axial force damping coefficients   | $C_{ZZ}, C_{Zf_Y}, C_{Zf_X}$   | $\bar{C}_{ZZ} = \frac{C_{ZZ} C \Omega}{F_*}, \bar{C}_{Zf_Y} = \frac{C_{Zf_Y} C \Omega}{F_* R_{out}}, \bar{C}_{Zf_X} = \frac{C_{Zf_X} C \Omega}{F_* R_{out}}$                                     |
| Axial force inertia coefficients   | $M_{ZZ}, K_{Zf_Y}, K_{Zf_X}$   | $\bar{M}_{ZZ} = \frac{M_{ZZ} C \Omega^2}{F_*}, \bar{M}_{Zf_Y} = \frac{M_{Zf_Y} C \Omega^2}{F_* R_{out}}, \bar{M}_{Zf_X} = \frac{M_{Zf_X} C \Omega^2}{F_* R_{out}}$                               |
| Moment stiffness coefficients      | $K_{f_Y Z}, K_{f_Y f_Y}, K_{f_Y f_X}$<br>$K_{f_X Z}, K_{f_Y f_X}, K_{f_X f_X}$ | $\bar{K}_{f_Y Z} = \frac{K_{f_Y Z} C}{F_* R_{out}}, \bar{K}_{f_Y f_Y} = \frac{K_{f_Y f_Y} C}{F_* R_{out}^2}, \bar{K}_{f_Y f_X} = \frac{K_{f_Y f_X} C}{F_* R_{out}^2}$                            |
| Moment damping coefficients        | $C_{f_Y Z}, C_{f_Y f_Y}, C_{f_Y f_X}$<br>$C_{f_X Z}, C_{f_Y f_X}, C_{f_X f_X}$ | $\bar{C}_{f_Y Z} = \frac{C_{f_Y Z} C \Omega}{F_* R_{out}}, \bar{C}_{f_Y f_Y} = \frac{C_{f_Y f_Y} C \Omega}{F_* R_{out}^2}, \bar{C}_{f_Y f_X} = \frac{C_{f_Y f_X} C \Omega}{F_* R_{out}^2}$       |
| Moment inertia coefficients        | $M_{f_Y Z}, M_{f_Y f_Y}, M_{f_Y f_X}$<br>$M_{f_X Z}, M_{f_Y f_X}, M_{f_X f_X}$ | $\bar{M}_{f_Y Z} = \frac{M_{f_Y Z} C \Omega^2}{F_* R_{out}}, \bar{M}_{f_Y f_Y} = \frac{M_{f_Y f_Y} C \Omega^2}{F_* R_{out}^2}, \bar{M}_{f_Y f_X} = \frac{M_{f_Y f_X} C \Omega^2}{F_* R_{out}^2}$ |

## Force and moment coefficients for the aligned hybrid thrust bearing

Table 3 details the predicted values of the bearing characteristics at the nominal clearance position,  $C=0.051$  mm, and without shaft misalignment. Note that for the aligned condition, the restoring moments are null, i.e.  $M_X=M_Y=0$ .

**Table 3. Bearing performance parameters at nominal operating clearance and aligned shaft collar.**

|   | <u>Symbol</u>   | <u>Dimensional value</u>  |
|---|---|---|
| Recess, minimum and maximum film pressures                          | $P_R, P_{min}, P_{max}$                                     | 19.81, 9.95, 23.175 bars  |
| Recess mass flow rate, mass flow rate through inner and outer radii | $M_R, M_{Rin}, M_{Rout}$                                    | 0.0588, 0.0567, 0.297 kg/s  |
| Axial load and torque   | $F_Z, T_o$  | 1374 N, 3.57 Nm   |
| Restoring Moments   | $M_X, M_Y$  | 0, 0 Nm   |
| Axial force stiffness coefficients                                  | $K_{ZZ}, K_{zf_y}, K_{zf_x}$                                | 41.3 MN/m, 0 N/rad, 0 N/rad   |
| Axial force damping coefficients                                    | $C_{ZZ}, C_{zf_y}, C_{zf_x}$                                | 29.4 kN s/m, 0 N s/rad, 0 N s/rad   |
| Axial force inertia coefficients                                    | $M_{ZZ}, K_{zf_y}, K_{zf_x}$                                | 2.36 Ns <sup>2</sup> /m, 0 N s <sup>2</sup> /rad, 0 N s <sup>2</sup> /rad                     |
| Moment stiffness coefficients                                       | $K_{f_x f_x} = K_{f_y f_y}$<br>$K_{f_x f_y} = -K_{f_y f_x}$ | 64.2 kN m/rad,<br>36.1 kN m/rad   |
| Moment damping coefficients   | $C_{f_x f_x} = C_{f_y f_y}$<br>$C_{f_x f_y} = -C_{f_y f_x}$ | 43.65 N m s/rad<br>6.25 N m s/rad   |
| Moment inertia coefficients   | $M_{f_x f_x} = M_{f_y f_y}$<br>$M_{f_x f_y} = -M_{f_y f_x}$ | $3.30 \cdot 10^{-3}$ N m s <sup>2</sup> /rad<br>$-0.19 \cdot 10^{-3}$ N m s <sup>2</sup> /rad |
| Other cross-force and moment coefficients                           |   | 0   |

San Andrés [2, 3] discusses the bearing performance for two operating speeds and increasing axial loads. Figure 3 reproduces some of the calculated axial load performance parameters for the statically aligned hybrid thrust bearing ( $f_x = f_y = 0$ ). Note that as the axial load increases, the recess pressure ( $\bar{P}_R$ ) increases towards the supply value and the operating (axial) clearance decreases rapidly. For the smallest load the maximum or largest clearance equals 101.6 microns. The dynamic force damping coefficient ( $\dot{C}_{ZZ}$ ) for axial motions remains more or less uniform for the range of small to moderate loads, and increases rapidly for heavily loaded conditions due to enhanced hydrodynamic effects. The static ( $\dot{K}_{ZZ}$ ) and synchronous ( $\dot{K}_{ZZ}$ - $\dot{M}_{ZZ}$ ) axial stiffness coefficients show a typical behavior with an optimum value for moderate loads at a recess pressure ratio ( $\bar{P}_R$ )  $\sim 0.6$ , as expected from a turbulent flow hydrostatic bearing.

Recall that at the statically aligned bearing condition,  $Z_{zf_x} = Z_{zf_y} = 0 = Z_{f_x z} = Z_{f_x y} = 0$ ; and  $Z_{f_x f_x} = Z_{f_y f_y}$ ;  $Z_{f_y f_x} = -Z_{f_x f_y}$ ; thus, the equivalent moment stiffness coefficient and

$$\text{whirl frequency ratio reduce to } K_{eq} = K_{f_x f_x} + K_{f_x f_y} \frac{C_{f_x f_y}}{C_{f_x f_x}}; \quad WFR = \frac{K_{f_x f_y}}{\Omega C_{f_x f_x}}.$$

Figure 4 depicts the moment coefficients for increasing axial loads. The static and (synchronous) dynamic direct coefficients ( $\bar{K}_{f_x f_x}$ ,  $\bar{K}_{f_x f_x} - \bar{M}_{f_x f_x}$ ) show a similar behavior as the axial force coefficients, i.e. render low values for small and large recess pressures and an optimum (maximum) value at about the same recess pressure for the axial force stiffness. On the other hand, the direct moment/angle damping ( $\bar{C}_{f_x f_x} = \bar{C}_{f_y f_y}$ ) and cross-stiffness ( $\bar{K}_{f_x f_y} = -\bar{K}_{f_y f_x}$ ) coefficients increase rapidly with the applied load, thus denoting the large influence of hydrodynamic effects as the operating clearance decreases. The whirl frequency ratio (*WFR*) is approximately 0.50 for all operating conditions, thus showing hybrid thrust bearings undergoing angular shaft motions have the same inherent stability limit as hydrodynamic thrust bearings and face seals.

### Effect of shaft static misalignment on thrust bearing performance

The following figures depict the effect of the shaft collar static misalignment angle ( $f_x$ ) on the performance characteristics of the hybrid thrust bearing operating with a nominal clearance of 0.51 mm [ $(\bar{P}_r) \sim 0.6$ ]. Recall that operation at this condition shows near optimum (direct) axial force and moment direct stiffness coefficients. The calculations were conducted for misalignment angles ( $f_x$ ) as large as 723 micro radians, which translate into a minimum film thickness as low as 10% of the nominal clearance.

Figures 5 through 7 show the predicted static performance characteristics of the hybrid thrust bearing. Minimum and maximum film pressures and recess pressures increase (nearly) linearly as the misalignment angle increases. The largest film and recess pressures are located on the side of the minimum film thickness. The maximum film pressure is already larger than the supply pressure for relatively small misalignment angles and denotes the dominance of centrifugal hydrodynamic flow effects as noted earlier in [2]. The minimum film pressures are lower than the bearing discharge pressure due to fluid inertia effects as also discussed then<sup>2</sup>.

Figure 6 depicts the dimensionless mass flow rates through the inner and outer radii of the bearing versus the misalignment angle. Again, due to centrifugal fluid inertia effects, the flow rate leaving the bearing through the inner radius decreases as the misalignment

<sup>2</sup> The dimensionless pressure corresponding to the refrigerant saturation pressure equals  $-0.405$ . Thus, the predictions indicate zones of fluid cavitation (vaporization), in particular at the downstream side of a recess in the circumferential direction.

angle increases (minimum film thickness decreases). There is approximately a 20% reduction in flow rate ( $M = \dot{M}_{Rout} + \dot{M}_{Rin}$ ) from the nominal condition to that with the largest misalignment angle.

Figure 7 shows the predicted axial force ( $\bar{F}_z$ ), drag torque ( $\bar{T}_o$ ) and restoring moments ( $\bar{M}_x, \bar{M}_y$ ) versus the misalignment angle ( $f_x$ ). The axial force and drag torque remain relatively insensitive to the degree of misalignment while the restoring moments increase rapidly. The rate of growth of the hydrostatic reaction moment ( $\bar{M}_x$ ) appears to be linear with the misalignment angle, while the cross-moment ( $\bar{M}_y$ ) due to hydrodynamic effects is of importance at large misalignment angles.

Figures 8 and 9 depict the dimensionless force stiffness and damping coefficients due to shaft axial displacements and angulations, respectively. As the misalignment angle ( $f_x$ ) increases, the axial force stiffness and damping coefficients ( $\bar{K}_{zz}, \bar{C}_{zz}$ ) due to shaft axial displacements are larger (though relatively invariant) than the force coefficients ( $\bar{K}_{zf_x}, \bar{C}_{zf_x}$ ) and ( $\bar{K}_{zf_y}, \bar{C}_{zf_y}$ ) due to shaft angulations. However, for large misalignment angles the cross-coefficients ( $\bar{K}_{zf_y}, \bar{C}_{zf_x}$ ) due to hydrodynamic effects become important.

Figures 10 and 11 show the dimensionless moment stiffness and damping coefficients due to shaft angulations and axial displacements, respectively. The direct moment-angle coefficients are significant for an aligned shaft condition while the cross-moment coefficients are negligible. Note that the symmetry (anti-symmetry) relations hold at the aligned condition. The direct moment stiffness coefficients ( $\bar{K}_{f_x f_x}, \bar{K}_{f_y f_y}$ ) remain relatively constant even for large misalignment angles, while the cross-stiffnesses ( $\bar{K}_{f_x f_y}, -\bar{K}_{f_y f_x}$ ) are smaller and increase rapidly due to the hydrodynamic shear flow effect. The direct moment damping coefficients ( $\bar{C}_{f_x f_x}, \bar{C}_{f_y f_y}$ ), always larger than the cross-damping coefficients ( $\bar{C}_{f_x f_y}, -\bar{C}_{f_y f_x}$ ), increase rapidly as the misalignment angle grows since the local film thickness is smaller. Note also that the hydrodynamic moment stiffness ( $-\bar{K}_{f_x z}$ ) and damping ( $\bar{C}_{f_x z}$ ) coefficients due to shaft axial displacements increase rapidly for large misalignment angles.

The predicted whirl frequency ratio ( $WFR = \frac{w_n}{\Omega}$ ) for a shaft collar undergoing dynamic angulations remains uniform at approximately 0.50 for most misalignment angles. The equivalent moment stiffness ( $\bar{K}_{eq}$ ), here mainly determined by the hydrostatic stiffnesses ( $\bar{K}_{f_x f_x} \sim \bar{K}_{f_y f_y}$ ), provides a measure of the largest mass moment of inertia for safe operation of the rotating system, i.e.  $I = \frac{K_{eq}}{w_n^2}$  without the likelihood of a hydrodynamic instability.

The predictions presented correspond to a bearing with axial injection at the mid plane of a recess. Calculations were also performed for hydrostatic feed with a tangential feed injection (90 degrees) opposite to the shaft rotational speed and at different circumferential locations upstream and downstream of a recess. These predictions were conducted to determine if the whirl frequency ratio would decrease so as to render a more robust bearing free of hydrodynamic instability. Table 4 below shows the predicted results for the axial force, torque, force and moment coefficients for the bearing aligned condition at the nominal operating condition ( $C=0.051$  mm).

**Table 4. Predictions for aligned bearing with angled hydrostatic feed injection.**

| Feed angle degrees | Position | $F_Z$<br>kN | $T_o$<br>Nm | $K_{ZZ}$<br>MN/m | $C_{ZZ}$<br>KNs/m | $K_{f_x f_x}$<br>KNm/rad | $K_{f_x f_y}$<br>KNm/rad | $C_{f_x f_x}$<br>Nm.s/rad | $C_{f_x f_y}$<br>Nm.s/rad | $K_{eq}$<br>KNm/rad | WFR  |
|--------------------|----------|-------------|-------------|------------------|-------------------|--------------------------|--------------------------|---------------------------|---------------------------|---------------------|------|
| 0                  | 0.5      | 1.37        | 3.56        | 41.3             | 29.4              | 64.1                     | 36.1                     | 43.6                      | 6.25                      | 69.6                | 0.50 |
| 90                 | 0.1      | 1.41        | 3.50        | 45.2             | 30.8              | 70.8                     | 35.6                     | 45.7                      | 5.88                      | 75.3                | 0.46 |
| 90                 | 0.5      | 1.39        | 3.34        | 40.7             | 29.9              | 64.2                     | 32.6                     | 43.4                      | 5.42                      | 68.3                | 0.44 |
| 90                 | 0.9      | 1.45        | 3.23        | 37.3             | 27.7              | 59.4                     | 29.7                     | 41.2                      | 4.93                      | 62.8                | 0.43 |

Angle: 0 = axial feed, +90 degrees = tangential against shaft rotation, -90 degrees = tangential parallel to shaft rotation  
 Position: 0.5 = middle of recess, 0.0 = upstream edge of recess, 1.0 = downstream edge of recess.

The predictions show that angled injection reduces slightly the whirl frequency ratio but not significantly to free the bearing from its limited stability limit. Note that this bearing application has large surface speeds with a nominal circumferential flow Reynolds number approximately equal to 33,000; thus then the limited advantage of angled injection. Similar results (theoretical and experimental) have been obtained for radial hydrostatic bearings [9]. Nonetheless note that a hybrid bearing with a tangential injection orifice location well upstream within the recess (position 0.1) shows a significant increase for its equivalent angular stiffness ( $K_{eq}$ ), thus effectively increasing the critical mass moment of inertia of the rotating system. On the other hand, tangential feed injection located well downstream of the recess (position 0.9) shows a significant reduction in the cross-coupled stiffness coefficient  $K_{f_x f_y}$ ; thus rendering the lowest whirl ratio but also the lowest equivalent angular stiffness. The predictions also show that the axial load and axial force displacement coefficients ( $K_{ZZ}$ ,  $C_{ZZ}$ ) are not greatly affected by the angled feed injection.

## CONCLUSIONS

A bulk-flow analysis and computer program for prediction of the static load performance and dynamic force and moment coefficients of angled injection, orifice-compensated hydrostatic / hydrodynamic thrust bearings have been completed. Advanced cryogenic fluid turbopumps are very compact, operate at extremely high shaft speeds, and require of hybrid (hydrostatic / hydrodynamic) radial and thrust fluid film bearings for accurate rotor positioning and control of critical speeds.

The analysis accounts for the bulk-flow mass, momentum and thermal energy transport, includes flow turbulence and fluid inertia (advection and centrifugal) effects on film lands and recesses, and incorporates cryogenic fluid properties using a NIST data base. The computer program predicts the flow rate, load capacity, restoring moments, power loss and 27 dynamic force coefficients for rigid surface, tapered land hybrid thrust bearings.

Predictions on the effects of shaft collar misalignment on the static and dynamic force and moment performance of a refrigerant R134a hybrid thrust bearing are presented. The axial force stiffness coefficient and the direct moment/angle stiffness coefficients show an optimum value for a certain load (recess pressure ratio) while the damping coefficient steadily increases with the applied load. As the misalignment angle increases, both moment and force coefficients due to shaft axial displacements and angulations also increase. The most important result is, however, the prediction of a whirl frequency ratio equal to 0.50 for most operating conditions. That is, thrust hybrid bearings offer the same limited stability characteristics as hydrodynamic bearings thrust when undergoing self-excited shaft angular motions.

The research conducted concludes a multiple year effort funded by NASA Centers for the development of sound computational tools able to predict reliably the performance of externally pressurized bearings needed for their current state of the art turbo pump technology.

## REFERENCES

- [1]. Pinkus, O., and J.K. Lund, 1981, "Centrifugal Effects in Thrust Bearings Under Laminar Conditions," *ASME Journal of Lubrication Technology*, Vol. 103, pp. 126-136.
- [2]. San Andrés, L., 1998, "Bulk Flow Analysis of Hybrid Thrust Bearings for Advanced Cryogenic Turbopumps", FINAL Technical Report to NASA Marshall Space Flight Center, NASA Grant NAG8-1395, October.
- [3]. San Andrés, L., "Bulk-Flow Analysis of Hybrid Thrust Bearings for Process Fluid Applications," *ASME Journal of Tribology*, Vol. 122, 1, pp. 170-180, 2000.
- [4]. McCarty, R.D., NBS Standard Reference Data Base 12, 1986, "Thermophysical Properties of Fluids, MIPROPS86," National Bureau of Standards, Colorado.
- [5]. San Andrés, L., "The Effect of Journal Misalignment on the Operation of a Turbulent Hydrostatic Bearing," *ASME Journal of Tribology*, Vol. 115, 3, pp. 355-363, 1993.
- [6]. San Andrés, L., 1995, "Thermohydrodynamic Analysis of Fluid Film Bearings for Cryogenic Applications," *AIAA Journal of Propulsion and Power*, Vol. 11, No. 5, pp. 964-972.
- [7]. Launder, B. E., and Leschziner, M., 1978, "Flow in Finite-Width Thrust Bearings Including Inertial Effects. – 2-Turbulent Flow," *ASME Journal of Lubrication Technology*, Vol. 100, pp. 339-345.
- [8]. Van Doormaal, J. P., and Raithby, G. D., 1984, "Enhancements of the SIMPLE Method for Predicting Incompressible Fluid Flows," *Numerical Heat Transfer*, Vol. 7, pp. 147-163.
- [9]. San Andrés, L., and D. Childs, 1997, "Angled Injection - Hydrostatic Bearings, Analysis and Comparison to Test Results," *ASME Journal of Tribology*, Vol. 119, 1, pp. 179-187.

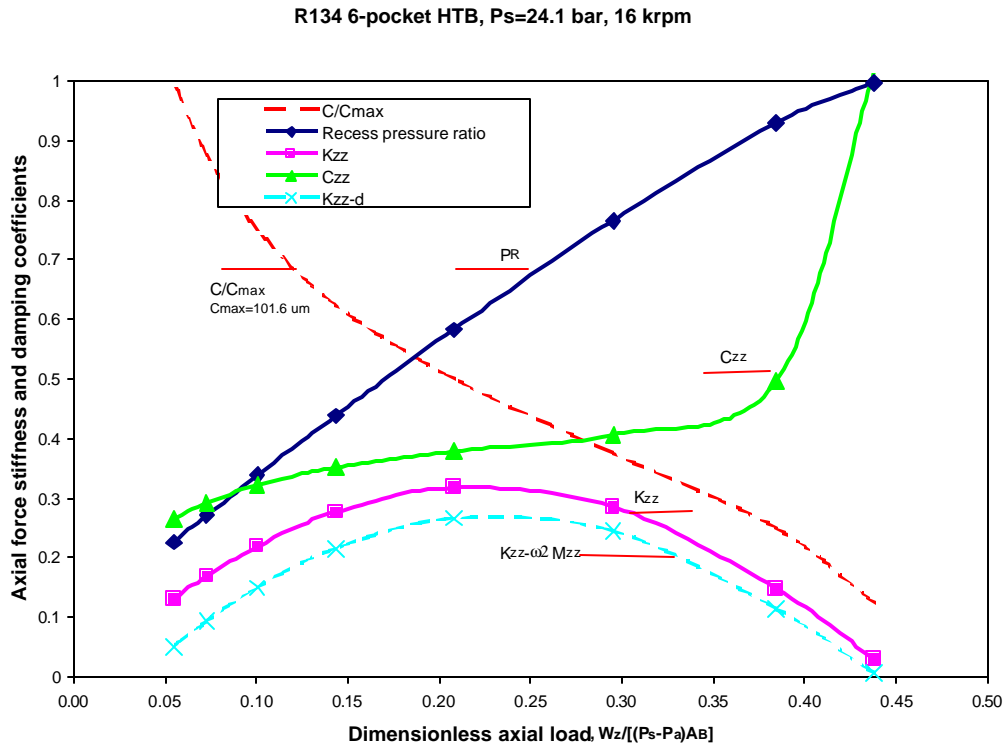


Figure 3. Operating clearance, recess pressure ratio, and axial force coefficients ( $K_{zz}$ ,  $C_{zz}$ ) versus axial load for statically aligned bearing.

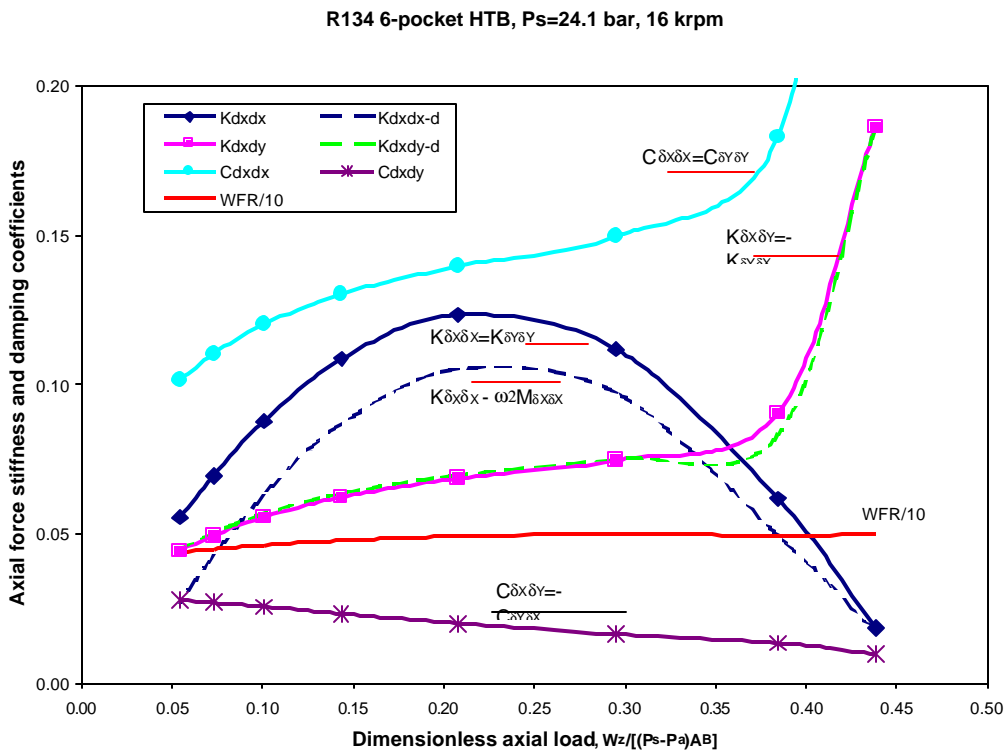


Figure 4. Moment force coefficients ( $K_{\delta_x \delta_x}$ ,  $K_{\delta_x \delta_y}$ ,  $C_{\delta_x \delta_x}$ ,  $C_{\delta_x \delta_y}$ ) and whirl ratio versus axial load for statically aligned bearing.

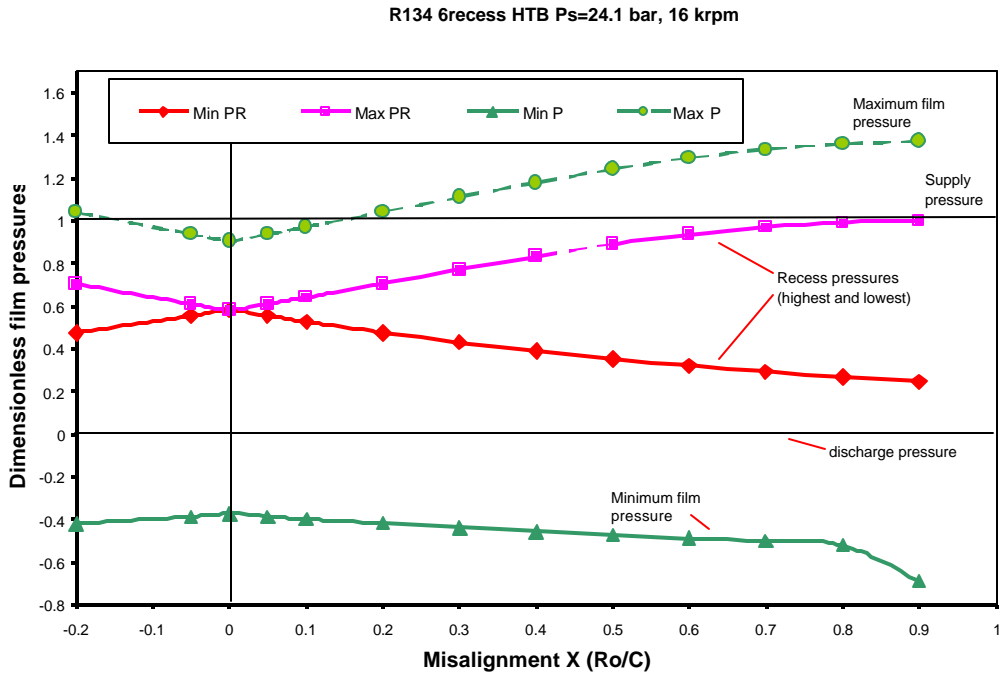


Figure 5. Minimum and maximum film and recess pressures versus shaft collar static misalignment angle -  $f_x R_{out} / C$ .

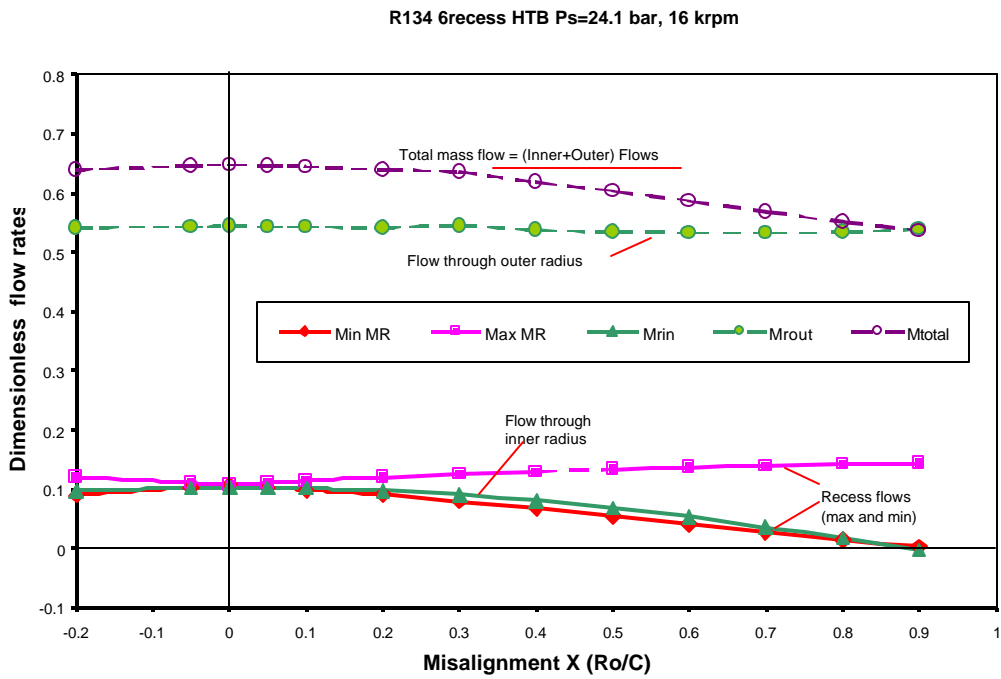


Figure 6. Mass flow rates through bearing inner and outer radii and recess flow rate versus shaft collar static misalignment angle -  $f_x R_{out} / C$ .

R134 6recess HTB Ps=24.1 bar, 16 krpm

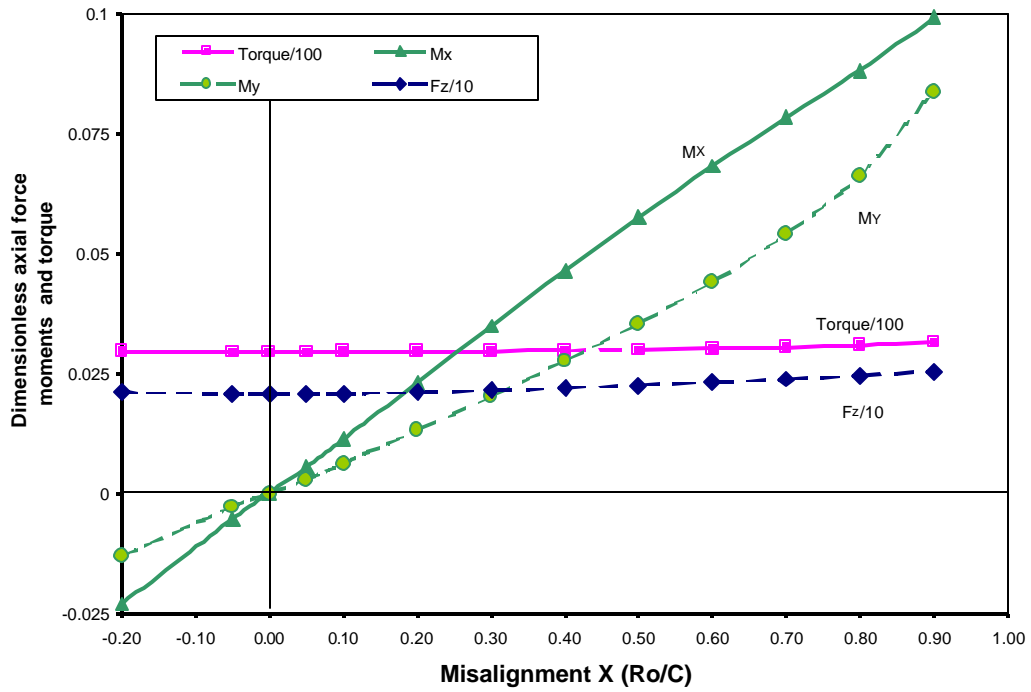


Figure 7. Axial load ( $F_z$ ), drag torque ( $T_o$ ) and restoring moments ( $M_x, M_y$ ) versus shaft collar static misalignment angle -  $f_x R_{out} / C$ .

R134 6recess HTB Ps=24.1 bar, 16 krpm

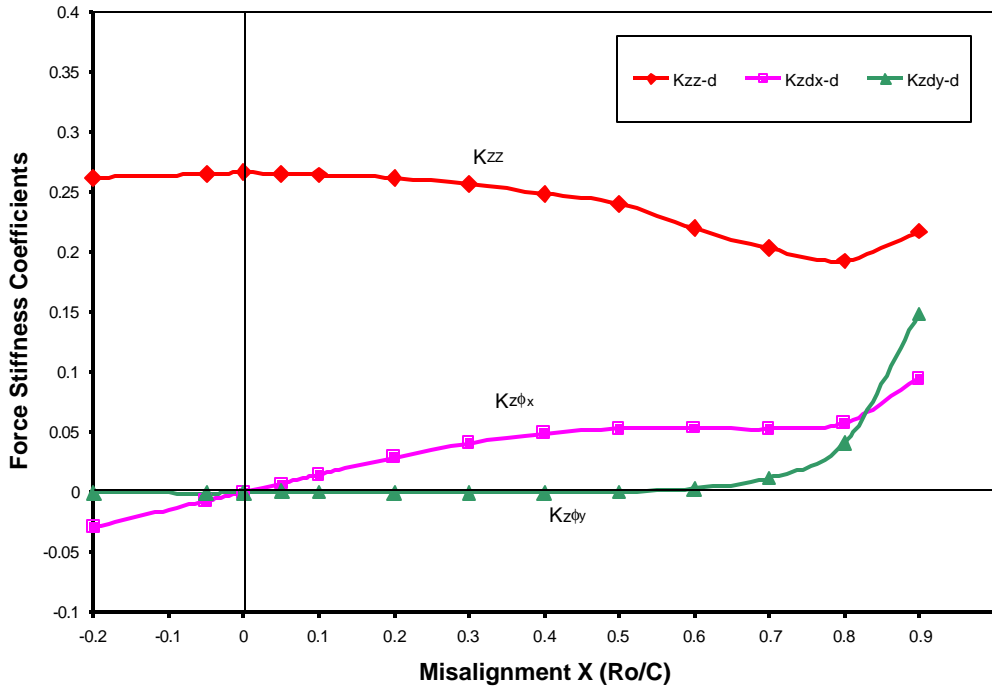


Figure 8. Synchronous (force) stiffness coefficients versus shaft collar static misalignment angle -  $f_x R_{out} / C$ .

R134 6recess HTB Ps=24.1 bar, 16 krpm

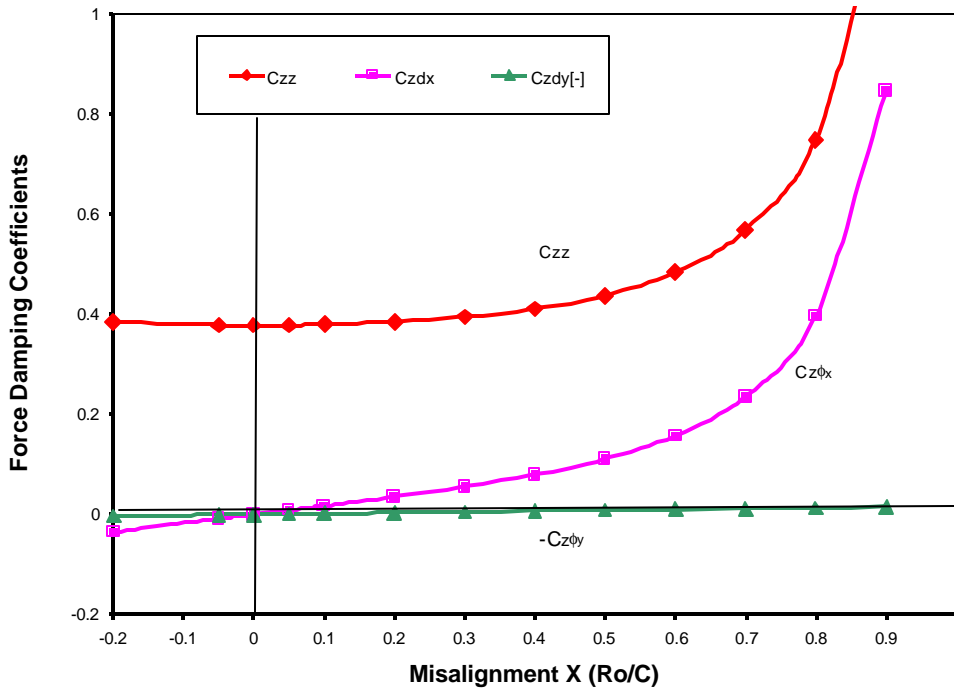


Figure 9. Force damping coefficients versus shaft collar static misalignment angle -  $f_x R_{out} / C$ .

R134 6recess HTB Ps=24.1 bar, 16 krpm

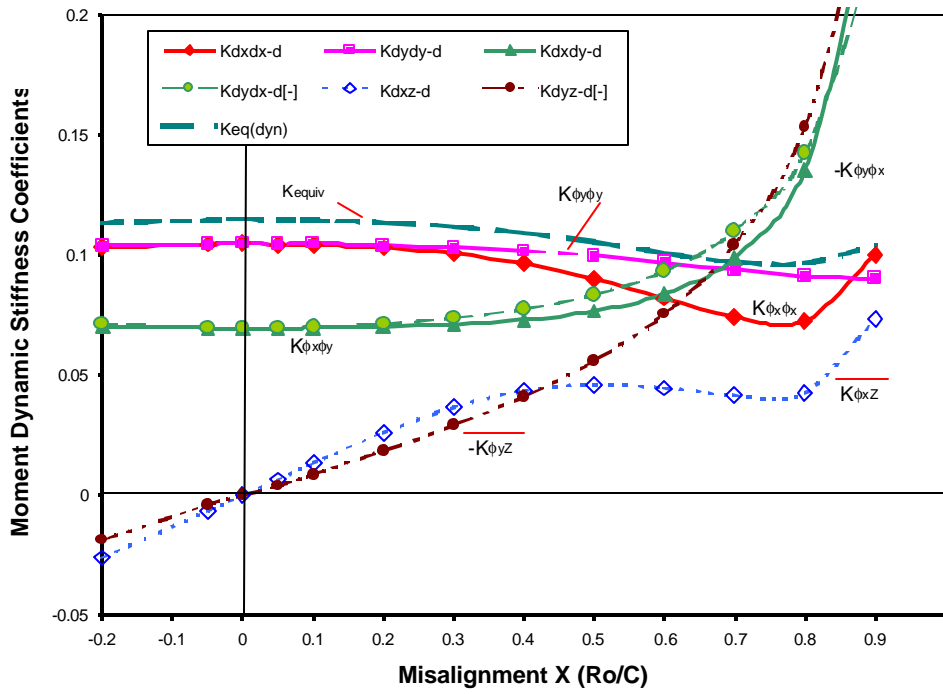


Figure 10. Synchronous moment stiffness coefficients versus shaft collar static misalignment angle -  $f_x R_{out} / C$ .

R134 6recess HTB Ps=24.1 bar, 16 krpm

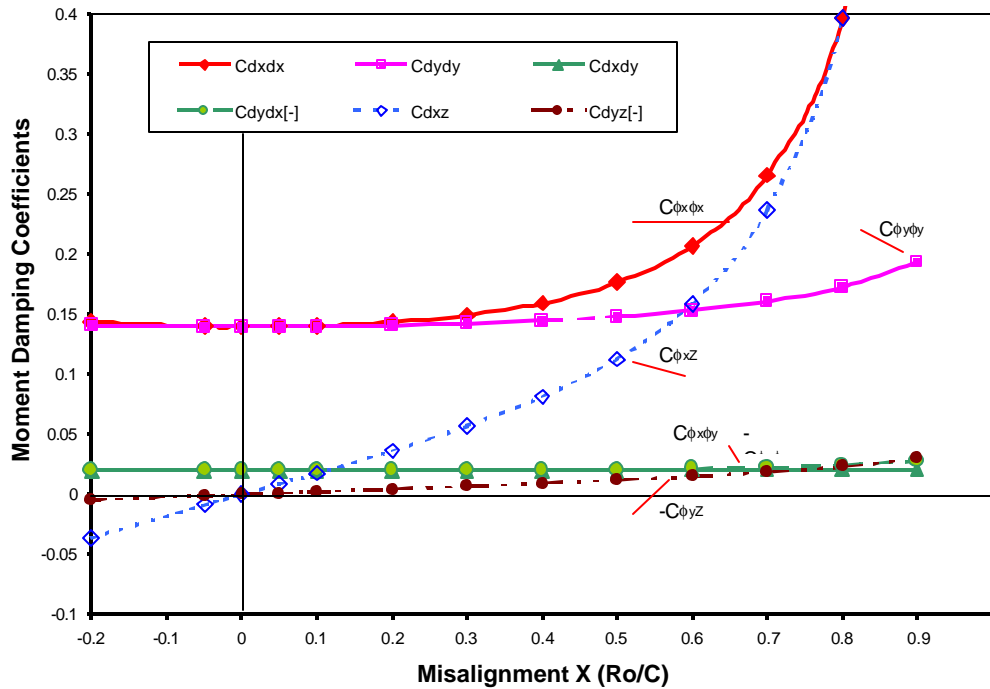


Figure 11. Moment damping coefficients versus shaft collar static misalignment angle -  $f_x R_{out} / C$ .

